EINDHOVEN UNIVERSITY OF TECHNOLOGY

Trap-Assisted Charge Generation and Recombination in State-of-the-Art Organic Photodetectors

Citation for published version (APA):
Ma, X., Janssen, R. A. J., & Gelinck, G. H. (2023). Trap-Assisted Charge Generation and Recombination in State-of-the-Art Organic Photodetectors. *Advanced Materials Technologies*, *8*(16), Article 2300234. https://doi.org/10.1002/admt.202300234

DOI:
10.1002/admt.202300234

Document status and date:
Published: 25/08/2023

Document Version:
Publisher's PDF, also known as Version of Record (includes final page, issue and volume numbers)

Please check the document version of this publication:

• A submitted manuscript is the version of the article upon submission and before peer-review. There can be important differences between the submitted version and the official published version of record. People interested in the research are advised to contact the author for the final version of the publication, or visit the DOI to the publisher's website.
• The final author version and the galley proof are versions of the publication after peer review.
• The final published version features the final layout of the paper including the volume, issue and page numbers.

Link to publication

General rights
Copyright and moral rights for the publications made accessible in the public portal are retained by the authors and/or other copyright owners and it is a condition of accessing publications that users recognise and abide by the legal requirements associated with these rights.

• Users may download and print one copy of any publication from the public portal for the purpose of private study or research.
• You may not further distribute the material or use it for any profit-making activity or commercial gain
• You may freely distribute the URL identifying the publication in the public portal.

If the publication is distributed under the terms of Article 25fa of the Dutch Copyright Act, indicated by the "Taverne" license above, please follow below link for the End User Agreement:

www.tue.nl/taverne

Take down policy
If you believe that this document breaches copyright please contact us at:

openaccess@tue.nl

providing details and we will investigate your claim.

Download date: 05. Oct. 2023

Check for updates

Trap-Assisted Charge Generation and Recombination in State-of-the-Art Organic Photodetectors

*Xiao Ma, René A. J. Janssen, and Gerwin H. Gelinck**

The performance of organic photodetectors is steadily improving, and the specific detectivity, as a key figure of merit, has reached values of 10^{12}–10^{13} Jones, i.e., comparable to that of silicon diodes but still considerably lower than the intrinsic limit. As with other semiconductor devices, the electrical performance of state-of-the art organic photodiodes (OPDs) is presently determined to a high degree by the presence of chemical impurities or structural defects which create carrier trapping states within the bandgap of organic active layer. This review aims to provide a comprehensive and timely account of trap-assisted charge generation and recombination in OPDs, with emphasis on the impact of these phenomena on photodetector performance parameters such as, noise and dark current density, responsivity, response speed, and ultimately, specific detectivity.

1. Introduction

Organic photodiodes (OPDs) are very attractive for light sensing applications as they combine interesting optoelectronic properties and high photogeneration yield with low fabrication costs, lightweight and mechanical flexibility. OPDs are proposed for use in color scanners,[1,2] medical X-ray detectors,[3,4] and other (bio)medical imagers,[5] biometric fingerprint and palmprint scanners,[6,7] and optical communications.[8,9] With the development of novel photoactive materials, proper contact engineering and optimization of device processing, the performance of organic photodetectors has significantly increased over the last 5 years. Visible OPDs show performance on par with amorphous silicon photodiodes.[10] The synthesis of novel narrow-bandgap polymer donors[11–16] and nonfullerene acceptors (NFAs)[17–19] has successfully extended the spectral photon responses up to 900–1200 nm, a wavelength region where now expensive InGaAs detectors are being used commercially.

Highestestate-of-the-art OPDs are based on a bulk heterojunction (BHJ) architecture using an electron donor and acceptor material as a photoactive layer. Both materials are finely intermixed throughout the bulk of the photoactive film. The film is typically a few hundred nanometers thick. Photoexcited electron–hole pairs can dissociate efficiently at the donor–acceptor junction. **Figure 1**a shows a typical OPD architecture comprising a BHJ layer sandwiched between two electrodes modified with electron and hole transport layers (ETL and HTL). Its band diagram under reverse bias is shown in Figure 1b. Electron transport takes place in the acceptor phase to the cathode. Similarly, hole transport takes place in the donor phase to the anode. The effective bandgap of a BHJ diode can thus be defined as the energy difference between the Lowest Unoccupied Molecular Orbital (LUMO energy of the acceptor material and the Highest Occupied Molecular Orbital (HOMO) energy of the donor. The optical bandgap in these devices is determined by the material with the lowest HOMO–LUMO energy difference, being either the donor or acceptor material. The current density–voltage (J–V) characteristic of an organic bulk-heterojunction OPD is schematically shown in Figure 1c. Among others, two relevant parameters for OPDs are the photocurrent density (J_{ph}, SI units: A m^{-2}) and the noise current spectral density in dark, S_n (SI units: A Hz$^{-1/2}$). S_n should be minimized while the photoresponse—for a given light intensity—should be as high as possible. The two parameters are combined into a single figure of merit, the specific detectivity D^* defined as $D^* = R(\lambda)\sqrt{A}/S_n$, where the responsivity $R(\lambda)$ is the ratio between the generated J_{ph} and the irradiance (P, SI units: W m^{-2}) at a particular wavelength λ, and A the area of the photodetector (unit: cm^2). The common unit of D^* is cm^2 Hz$^{1/2}$ W^{-1} or Jones. Figure 1d shows reported D^* values of state-of-the-art OPDs, extracted from the literature, as a function wavelength corresponding to the optical bandgap. More details can be found in Tables S1 and S2 (Supporting Information). The empty blue symbols in Figure 1d represent D^* calculated from the reverse dark current, i.e., only considering shot noise, and

X. Ma, R. A. J. Janssen, G. H. Gelinck
Molecular Materials and Nanosystems and Institute for Complex Molecular Systems
Eindhoven University of Technology
P.O. Box 513, Eindhoven 5600 MB, The Netherlands
E-mail: gerwin.gelinck@tno.nl

R. A. J. Janssen
Dutch Institute for Fundamental Energy Research
De Zaale 20, Eindhoven 5612 AJ, The Netherlands

G. H. Gelinck
TNO/Holst Centre
High Tech Campus 31, Eindhoven 5656 AE, The Netherlands

The ORCID identification number(s) for the author(s) of this article can be found under https://doi.org/10.1002/admt.202300234

© 2023 The Authors. Advanced Materials Technologies published by Wiley-VCH GmbH. This is an open access article under the terms of the Creative Commons Attribution License, which permits use, distribution and reproduction in any medium, provided the original work is properly cited.

DOI: 10.1002/admt.202300234

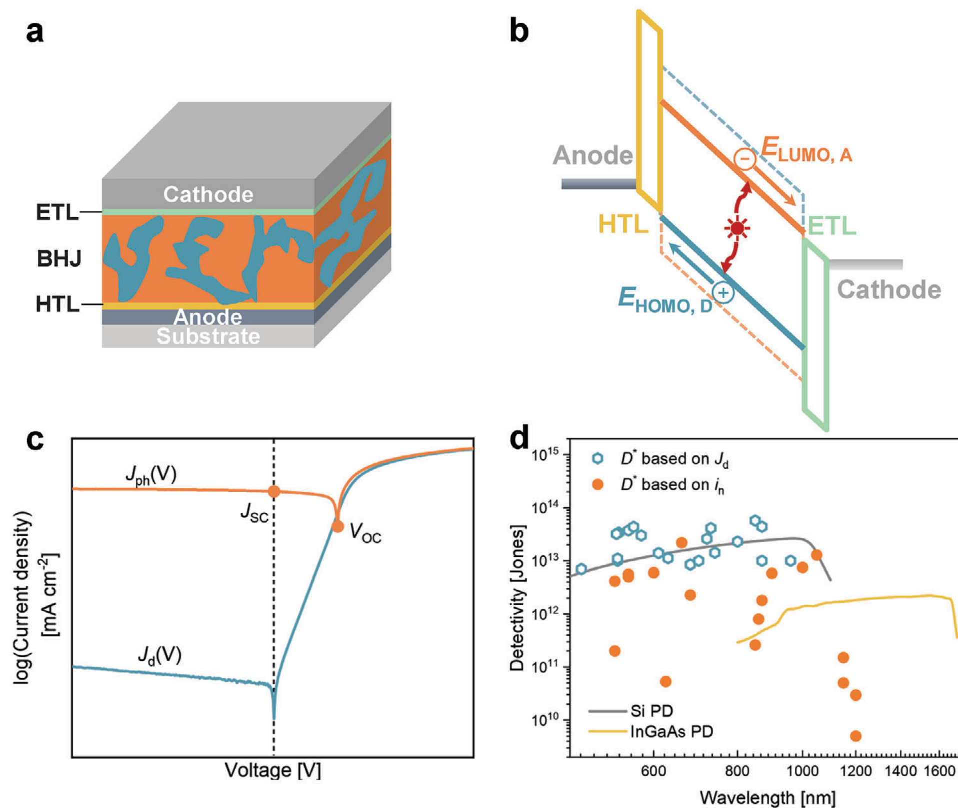

Figure 1. a) Schematic of an OPD consisting of bulk heterojunction (BHJ) layer between two electrodes modified with charge transport layers, a hole transport layer (HTL) and an electron transport layer (ETL). At least one of the electrodes is optically transparent. b) Band diagram under reverse bias. c) Schematic of OPD current density–voltage (J–V) characteristics with and without illumination. Dark current density (J_d), short-circuit photocurrent density (J_{sc}), and open-circuit voltage (V_{oc}) and are indicated. d) Reported specific detectivity of OPDs as a function of wavelength. Solid symbols represent D* calculated from i_n and empty symbols represent D* calculated from J_d. The device performance of the commercial inorganic photodiodes, Si (Thorlabs FDS100-CAL) and InGaAs (Thorlabs FGA21-CAL) are also included as reference. Further details about the individual devices are given in Tables S1 and S2 (Supporting Information).

the solid orange symbols represent reported D* calculated from measured noise current.

The ultimate performance of any light detector is achieved when the detector noise is low compared to the photon noise, i.e., the detector is “quantum limited.” Photon noise is fundamental. It directly follows from the discrete nature of the impinging photons including background radiation. Detector noise is unavoidable and related to fluctuations in charge carrier density and mobility. The ultimate limit of the specific detectivity is called the background-limited infrared photodetection (BLIP) limit, where D* is limited by the noise associated with photons from background radiation. The BLIP limit is calculated by using the black body radiation (which is strongly temperature dependent), assuming unit external quantum efficiency (EQE = 1), and a dark generation-recombination current that is only limited to radiative transitions over the bandgap of the semiconductor.[20,21] At 300 K, the BLIP detectivity value for a detector with a bandgap energy of 0.8 eV, corresponding to wavelengths up to 1550 nm, is $\approx 1 \times 10^{15}$ Jones. It increases strongly with decreasing wavelength.[15]

Three trends are observed in Figure 1d. First, all reported D* values fall short with respect to the BLIP limit, indicating that nonradiative transitions and losses are dominant. Second, detectivity values calculated using current noise are consistently lower than obtained using dark current density (J_d). This effect is well known: the calculation based on J_d assuming only a shot noise contribution is usually incorrect, and leads to an overestimation of D*.[20,22,23] Yet, best-in-class OPDs show noise current-based D* values comparable to that commercial inorganic PDs (gray and yellow line). Third, D* of OPDs with narrow bandgaps (i.e., $\lambda > 1100$ nm) are significantly smaller. The prime reasons are the reduced charge generation and enhanced charge recombination. Few donor:acceptor BHJs based on narrow bandgap organic semiconductors are known that produce charges when excited at wavelengths beyond 1100 nm,[11,18,24,25] or only when applying a sufficiently large reverse bias.[15,26] Moreover, charge recombination is enhanced in low-energy CT states. This is known as the “energy-gap law,”[27] which implies that nonradiative recombination becomes increasingly likely when the effective bandgap is reduced.[28] It is noted, however, that for modern donor—nonfullerene acceptor systems in which the locally excited (LE) state on the acceptor is degenerate with the CT state, nonradiative recombination is less strong, because radiative recombination is enhanced via intensity borrowing from the transition between the LE and ground state.[29,30] Next to reduced formation of collectable charges, the drop of D* at long wavelengths originates from the increased dark current noise.

© 2023 The Authors. Advanced Materials Technologies published by Wiley-VCH GmbH

2365709x, 2023, 16, Downloaded from https://onlinelibrary.wiley.com/doi/10.1002/admt.202300234 by Technical University Eindhoven, Wiley Online Library on [06/09/2023]. See the Terms and Conditions (https://onlinelibrary.wiley.com/terms-and-conditions) on Wiley Online Library for rules of use; OA articles are governed by the applicable Creative Commons License

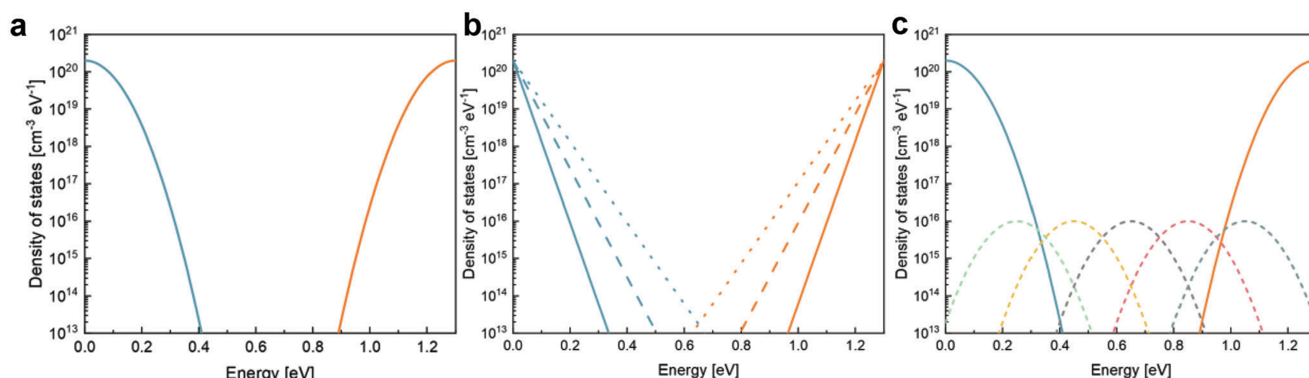

Figure 2. Simplified density of states diagram for an organic semiconductor with a gap energy E_g and different intra-bandgap states. a) Equal shapes of (broadened) HOMO and LUMO levels with a Gaussian width of 0.1 eV. b) Exponential tail states $\exp(E/E_0)$ for a value of E_0 of 20 meV (solid lines), 30 meV (dashed lines), and 40 meV (dotted lines). c) Deep discrete states with Gaussian distribution at trap depths from 0.25 to 1.05 eV, in steps of 0.20 eV. The peak heights, $N_{T,max}$, is 10^{16} cm^3 eV^{-1}, and the width of the Gaussian is 0.1 eV. For comparison, the Gaussian disordered HOMO and LUMO of a) are also included in (c).

Impurities, defects and charge trapping related phenomena in organic semiconductors are currently topics of intensive research, as they have frequently been reported to compromise the performance of organic light-emitting diodes, transistors, and organic solar cells.[31–33] Organic photodetectors are no exception. Recent reports have highlighted the negative impact of intra-bandgap electronic states on dark current, photoresponse, and response speed. This review focuses on OPDs and particularly the role of trap-mediated processes. It is organized as follows: In Section 2, we introduce the physical concepts on structural and energetic disorder in organic semiconductors that result in the presence of shallow and deep intra-bandgap states. In Section 3, we will introduce the relevant concepts that explain how such intra-bandgap states result in charge traps affecting charge transport and recombination processes. Sections 4, 5, and 6 give an overview of electronic and optical characterization methods used to characterize trap distribution in organic semiconductor diodes, including recent experimental and modeling results that clearly show that small amounts of deep energetic states at low density ($< 10^{16}$ cm^{-3}) have a profound negative impact on detectivity, photocurrent linearity and response time. Section 7 presents a short summary of the major findings and a short outlook in the form of recommendations in relation to accurate extraction of relevant photodetector parameters and trap state analysis.

2. Shallow and Deep Traps in Organic Semiconductors

Organic semiconductors belong to the class of so-called disordered semiconductors. Large electron–phonon interactions give rise to charge localization and a thermally assisted charge transport mechanism[34,35] in which holes or electrons hop from one molecule (or conjugated segment in case of a polymer) to another. Due to variations in packing, conformation, and local polarization, the density of states at HOMO and LUMO energies broaden. As a consequence of energetic and structural disorder, thermal activation energies of ≈0.2–0.3 eV are typically observed for the charge carrier mobility. Chemical impurities and defects can also lead to the formation of discrete electronic states in the forbidden energy gap of the organic semiconductor. Charge carriers can be immobilized in such a localized "trap state" when their relative energetic positions from the transport levels (trap depth) lies further than several kT, where k is Boltzmann's constant and T the absolute temperature, from the charge transport level.

The disorder inherent to organic semiconductors causes some of the in-band electronic states to tail into the bandgap and can be approximated by a Gaussian distribution at the HOMO and LUMO levels (**Figure 2**a). An exponential distribution tailing deeper into the bandgap is also often used. (Figure 2b). Band tails extending exponentially into the bandgap are mathematically expressed in the form of

$$N(E) = N_C \exp\left(-\frac{E_C - E}{E_{0,C}}\right), \quad E < E_C \tag{1}$$

where N_C is the density of states at the energy E_C of the conduction band edge (LUMO), and $E_{0,C}$ the characteristic decay energy of the band tail. There is a similar expression for the density of states near the valence-band edge (HOMO) with a characteristic energy $E_{0,V}$. For excitations below the bandgap the absorption coefficient decreases exponentially with decreasing photon energy. This absorption coefficient is believed to reflect the band-tail density of states. Most reported values of $E_{0,V}$ and $E_{0,C}$ range between 20 and 40 meV in best-of-class BHJ devices. Research spanning over more than a decade successfully links the disorder to the photovoltaic parameters of organic BHJ solar cells.[36–41] With typical E_0 numbers of 20–40 meV, Figure 2b shows that the density of states decreases rapidly into the bandgap. If there were no states in the gap other than these band tails, then the minimum density of states at mid-gap, using the value of 40 meV for the characteristic energies, N_C and N_V of 2×10^{20} cm^{-3} eV^{-1} and choosing an effective bandgap of 1.3 eV, which is typical for an OPD, would be $\approx 3 \times 10^{13}$ cm^{-3} eV^{-1}. This is an unrealistically small number, so we must conclude that other intra-bandgap states contribute in this region.

© 2023 The Authors. Advanced Materials Technologies published by Wiley-VCH GmbH

2365709x, 2023, 16, Downloaded from https://onlinelibrary.wiley.com/doi/10.1002/admt.202300234 by Technical University Eindhoven, Wiley Online Library on [06/09/2023]. See the Terms and Conditions (https://onlinelibrary.wiley.com/terms-and-conditions) on Wiley Online Library for rules of use; OA articles are governed by the applicable Creative Commons License

2365709x, 2023, 16, Downloaded from https://onlinelibrary.wiley.com/doi/10.1002/admt.202300234 by Technical University Eindhoven, Wiley Online Library on [06/09/2023]. See the Terms and Conditions (https://onlinelibrary.wiley.com/terms-and-conditions) on Wiley Online Library for rules of use; OA articles are governed by the applicable Creative Commons License

The origin of deep states (with trap depths >> kT) remained elusive for a long time. Charge traps have been attributed to morphological defects,[42–44] to chemical impurities remaining from materials' synthesis and device processing,[45–47] to contamination from the environment,[48] and light-induced material degradation.[49,50] An insightful study of Cowan et al. points to the role of molecular impurities.[50] The controlled introduction of one $PC_{84}BM$ molecule per 1000 $PC_{60}BM$ molecules—that act as electron trap sites with an energy of 0.35 eV—resulted already in a strong degradation in device performance. Such a molecular defect is likely to be described by a Gaussian trap distribution (Figure 2c).

3. How Intra-Bandgap States Influence Charge Transport and Generation-Recombination Processes

3.1. Diode Characteristics

The so-called ideal diode equation is an often-used starting point to describe the current–voltage characteristics of an organic BHJ photodiode

$$J = J_0 \left[\exp\left(\frac{qV}{n_{id}kT}\right) - 1\right] - J_{ph} \tag{2}$$

with q being the elementary charge, J_0 the reverse saturation current, and n_{id} is the ideality factor (in older literature referred to as quality factor). n_{id} equals unity in an ideal diode. In the dark, $J_{ph} = 0$, and Equation (2) can be written as

$$J_d = J_0 \left[\exp\left(\frac{qV}{n_{id}kT}\right) - 1\right] \tag{3}$$

The fundamentals of Equations (2) and (3) were laid by pioneers such as Shockley, Wright, and Rose. Shockley derived this equation for an inorganic p-n diode. Wright and Rose found that Equation (2) describes injection (dark) currents and photocurrents in diodes made from highly resistive (homo-junction) semiconductors. Wright[51] demonstrated that the single-carrier current in a device with one ohmic (injecting) contact and one blocking contact predominantly occurs by carrier diffusion at low forward bias, and increases exponentially with the applied voltage. The current at high forward bias becomes space-charge-limited current (SCLC) and can be described by the Mott–Gurney square law[52]

$$J = \frac{9}{8}\varepsilon\mu\frac{V^2}{L^3} \tag{4}$$

with ϵ the permittivity, μ the mobility, V the applied bias, and L the thickness of the active layer. From this equation, the space-charge limited charge-carrier mobility can be directly derived, provided care is taken to avoid caveats.[34,53] Trap-assisted processes result in a deviation of the ideal diode behavior, as will be shown next.

3.2. Charge Recombination

Recombination of photogenerated charges is an unwanted loss process in organic solar cells and photodetectors. A semiconductor at thermal equilibrium, i.e., without external voltage applied and in the dark, will have a recombination rate that is equal to the thermal generation rate. Understanding the physical processes governing charge recombination in these devices is therefore essential for improving their performance. Following Onsager–Braun's description[54,55] as well as more modern models, reviewed,[56] it is useful to consider recombination as a two-stage process, each being associated with a rate: the first process describes the probability that two oppositely charged carriers meet and form a pair of Coulomb-bound charges. This process can be reversible, i.e., the charge pair may dissociate again into independent mobile charges. The second stage describes the subsequent recombination of the Coulomb-bound charges. The overall rate is limited by the slowest process.

Despite clear physical mechanisms, charge recombination studies in BHJs initially led to seemingly conflicting results. The main reason is that the recombination mechanisms are mostly nonradiative in BHJ devices, and thus experimentally difficult to probe. Moreover, the kinetics of recombination strongly depend on charge density, and thus light intensity (due to photocarriers) and voltage (due to field-dependent drift of carriers, and injected dark carriers). Near open circuit recombination is dominated by interactions between free carriers or between a free carrier and a carrier in the tail state.[37,57] Understanding this better was of crucial importance for solar cell development.[58] At reverse bias or short-circuit conditions, bimolecular recombination is suppressed relative to monomolecular (trap-induced) recombination by the lower density of carriers and the relatively high electric field (V–V_{BI}), where V_{BI} is the built-in voltage resulting from the different work functions of the electrodes. This regime is more relevant for OPDs.

3.2.1. Bimolecular Recombination

In OPDs bimolecular recombination is often described in terms of the Langevin model, and extensions thereof.[34] According to this model, recombination occurs at every encounter of an electron and a hole. The rate limiting step is thus given by the diffusion of electrons and holes toward each other. The recombination rate (R_L) can be described as the product of the Langevin recombination coefficient and the excess charge density as

$$R_L = \frac{q}{\varepsilon_0\varepsilon_r}\left(\mu_e + \mu_h\right)\left(n_e n_h - n_i^2\right) \tag{5}$$

where μ_h and μ_e are the charge carrier mobility of holes and electrons, respectively, n_e and n_h are the (free) electron and hole density, ϵ_0 is the vacuum and ϵ_r is the relative permittivity, and n_i is the intrinsic carrier concentration. This rate increases quadratically with carrier density and therefore becomes more important at high light intensities.

3.2.2. Charge Transfer States at the BHJ Interface

The experimentally measured bimolecular recombination rate in BHJ solar cells has been found to be reduced with respect to Langevin rate. This leads to the introduction of an additional

 © 2023 The Authors. Advanced Materials Technologies published by Wiley-VCH GmbH

parameter γ as prefactor in Equation (6)

$$R_L = \gamma \frac{q}{\varepsilon_0 \varepsilon_r} \left(\mu_e + \mu_h\right) \left(n_e n_h - n_i^2\right) \tag{6}$$

The value of γ ranges between 10^{-1} and 10^{-3} in bulk heterojunction solar cells, and it decreases with increasing temperature.[58] The temperature-dependence of the reduction factor γ cannot be described by an encounter-limited recombination rate. This apparent contradiction was solved by assuming that the recombination process proceeds via a charge-transfer (CT) state formed at the interface.[59,60] The reduced Langevin recombination is hypothesized to result from an equilibrium between free carriers and populated CT states.[61] The fundamental assumption is that the CT states dissociate into free carriers several times before ultimately recombining.

3.2.3. Monomolecular (First Order) Recombination at the Contacts

Due to diffusion of charges from the contacts into the organic semiconductor (see also Section 4.3), a large charge imbalance can exist near the electrodes, e.g., a higher density of electrons at the cathode and a higher density of holes at the anode. Such an imbalance will enable mobile holes, n_h, to recombine in the presence of a significant excess of electrons, $n_{e,exc}$, via a seemingly first-order process: $R_{BI}^{1st} \propto n_{e,exc} \times n_h(P)$.[62–64] The first-order losses increase with decreasing carrier mobility.[65]

3.3. Trap-Assisted Recombination

Trap-assisted recombination is defined as a recombination process in which one electron and one hole recombine through a trap state or recombination center. First, fast initial capture of electrons (density, n_e) or holes (density, n_h) creates a finite concentration of trapped charges with which a mobile counter charge can recombine. The two-step mechanism transforms the recombination from a bimolecular process with incident light intensity, P, $R_{BI} \propto n_e(P) \times n_h(P)$, to a first-order process, $R_{SRH} \propto n_{e,trap} \times n_h(P)$.

Recombination through traps was first described by Shockley and Read[66] and independently by Hall,[67] and is known as Shockley–Read–Hall (SRH) recombination. The SRH model recognizes four pathways by which electrons and holes can recombine and re-establish the equilibrium that has been disturbed by thermal or photoexcitation:

1) an electron is captured by the trap
2) a trapped electron is thermally excited to the LUMO level
3) an electron is thermally excited to the trap from the HOMO level, i.e., hole emission from the trap
4) The trapped electron falls into an empty state near the valence band, i.e., hole capture.

Steps (1) and (4) taken together comprise a recombination event.

The net SRH recombination rate via traps of density N_t is given by[66–69]

$$R_{SRH} = \frac{C_n C_p N_t \left(n_e n_h - n_i^2\right)}{\left[C_n \left(n_e + n_1\right) + C_p \left(n_h + p_1\right)\right]} \tag{7}$$

with

$$n_1 = N_{LUMO} \exp\left(-\frac{E_{LUMO} - E_t}{kT}\right) \tag{8a}$$

$$p_1 = N_{HOMO} \exp\left(\frac{E_{HOMO} - E_t}{kT}\right) \tag{8b}$$

$$n_1 p_1 = N_{HOMO} N_{LUMO} \exp\left(-\frac{E_g}{kT}\right) \tag{8c}$$

in which $n_1 p_1 = n_i{}^2$, and E_g is the effective bandgap. The relevance of SRH recombination will therefore depend on the trap density, the trap energy (E_t), as well as the so-called capture coefficients C_n and C_p for electrons and holes, respectively. Equation (7) assumes steady-state condition (quasiequilibrium), i.e., the net rate between electron capture and electron emission ((1)−(2)) is equal to the net rate between hole capture and hole emission ((3)–(4)) in **Figure 3**a, which may not be the case in highly resistive semiconductors, with high bandgaps of 1.1 eV or higher.[34,70] It is more likely, because the recombination centers are near mid-gap, that equilibrium is determined by electron and hole capture rather than by thermal emission.

Figure 3a and Equations (7) and (8) represent the case of a single energy level located between the conduction band (HOMO) and valence band (LUMO), respectively. In disordered organic semiconductors, however, it is more likely that there is a broad distribution of intra-bandgap states that can act as trap of recombination center. For this case, the quasi-Fermi approach is much more useful and physically appealing.[71–73] Under illumination (or forward bias) a quasi-Fermi level for electrons $E_{f,n}$ is defined as the Fermi level consistent with a density n_e of free electrons following

$$n = N_C \exp\left(-\frac{E_C - E_{f,n}}{kT}\right) \tag{9a}$$

An analogous definition for the hole quasi-Fermi level $E_{f,p}$ yields density of holes n_h

$$p = N_V \exp\left(-\frac{E_{f,p} - E_V}{kT}\right) \tag{9b}$$

In a wide bandgap semiconductor, in the absence of illumination (or strong forward bias), these quasi-Fermi levels lie near mid-gap. Under illumination they move toward their respective mobility edges. As a first approximation, states lying between a mobility edge and a respective Fermi level act mainly as traps rather than as recombination centers. States lying between the two Fermi levels will be recombination centers. $E_{f,n}$ and $E_{f,p}$ energy levels therefore separate recombination from trapping effects, and therefore are sometimes referred to as the electron and hole demarcation level. An electron at this level will have the same probability of being thermally excited to the transport level as of capturing a hole.[74] States above this electron demarcation level D_n will act predominantly as traps, those below as recombination centers. Rose showed that (with a small correction factor that is negligible when the capture coefficients for hole and electron capture are identical) the demarcation level is located at the steady-state quasi-Fermi level.[72] These demarcation levels are

© 2023 The Authors. Advanced Materials Technologies published by Wiley-VCH GmbH

2365709x, 2023, 16, Downloaded from https://onlinelibrary.wiley.com/doi/10.1002/admt.202300234 by Technical University Eindhoven, Wiley Online Library on [06/09/2023]. See the Terms and Conditions (https://onlinelibrary.wiley.com/terms-and-conditions) on Wiley Online Library for rules of use; OA articles are governed by the applicable Creative Commons License

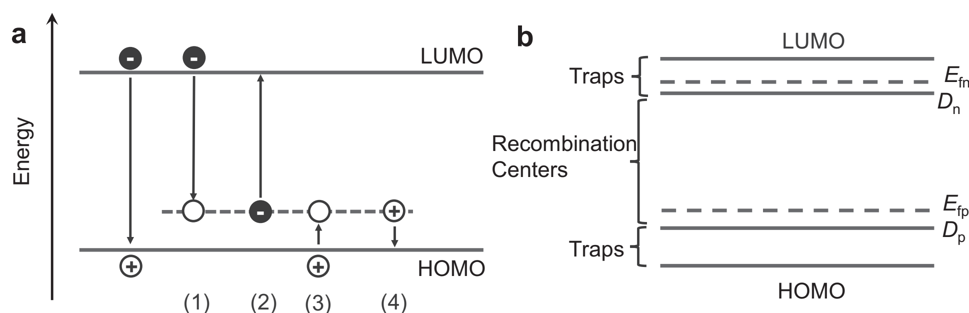

Figure 3. a) Schematic representation of bimolecular recombination and four processes involving recombination via trap states. 1) an electron is captured by the trap, 2) a trapped electron is thermally excited to the LUMO, i.e., electron emission, 3) a hole is captured by the trap, and 4) the trapped hole falls into an empty state near the valence band, i.e., hole emission. Adapted with permission.[75] Copyright 2011, American Institute of Physics. b) Band diagram to represent the demarcation levels D_n and D_p for electrons and holes, respectively. The quasi-Fermi levels for electrons and holes, respectively, are $E_{f,n}$ and $E_{f,p}$.

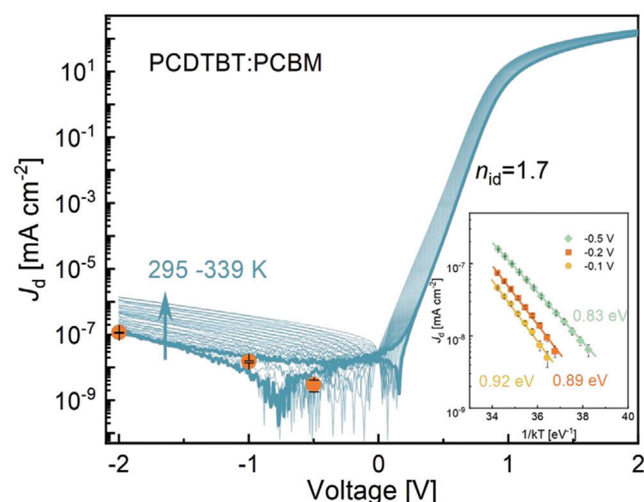

Figure 4. Dark current of PCDTBT:PCBM OPD at various temperatures. Lines represent forward and backward voltage scans. Bold lines represent room temperature data (295 K). Orange symbols represent current density values obtained under constant voltage conditions (at room temperature). Ideality factor of 1.7 was calculated using Equation (13). The inset shows the temperature dependence of J_d measured at different voltages. The dotted lines are Arrhenius-type fits with an activation energy E_a of 0.92 eV (at −0.1 V), 0.89 eV (at −0.2, and 0.82 eV (at −0.5 V). Reproduced under the terms of the Creative Commons Attribution 4.0 International license.[76] Copyright 2022, The Authors, published by Wiley–VCH GmbH.

represented in Figure 3b on a standard band diagram. All the states between D_n, and D_p are recombination centers, because the probability of thermal emission to a mobility edge is weak compared with electron or hole capture. Since the demarcation level is determined by the values of capture probabilities and recombination times, each different type of trap should have its own set of demarcation levels associated with it.

4. Charge Transport in Organic Semiconductor Diodes in Dark

Temperature-dependent *J*–*V* characteristics of a polymer-fullerene BHJ OPD in dark are shown in **Figure 4**. This particular polymer blend, consisting of poly[*N*-9′-heptadecanyl-2,7-carbazole-alt-5,5-(4′,7′-di-2-thienyl-2′,1′,3′-benzothiadiazole)] (PCDTBT) and phenyl-C_{61}-butyric acid methyl ester (PCBM), was used in two different prototypical photoimaging applications by our group.[4,6] It was also used in a recent device study by our group.[76] In this work, it serves as an illustrative example. Three voltage regimes can be discerned: i) at high positive voltage ($V > V_{BI}$) the electric field becomes positive, charges are injected, and the drift current density dominates. In this region, the current density can be described by the Parmenter and Ruppel model (see Section 4.2) and at high current densities series resistance may become important, ii) at low forward bias (from 0 V to V_{BI}) the current exhibits exponential diode characteristics due to the charge diffusing from the contacts into the semiconductor. In this regime, the drift-current density from injected chare carriers is still negative, but the gradient of charge carriers results in a diffusion of charges in the opposite direction. iii) at reverse bias (<0 V) currents are low, and in an ideal diode current, approaches the reverse saturation current (J_0) also known as the “thermal (or equilibrium) recombination current.”[77]

The solid lines in Figure 4 represent current densities measured in forward and backward voltage scans. The symbols represent J_d values measured at constant applied voltages, effectively eliminating displacement and charging currents.[76]

4.1. Trap-Limited Charge Transport Studies

The impact of trap states on charge carrier transport in organic diodes is well understood in single carrier (electron-only or hole-only) organic diodes. In these devices by proper contact engineering only one type of charge carrier is injected, and charge recombination can be neglected. The presence of deep trap states leads to deviation from the expected SCLC behavior. Traps effectively immobilize charge carriers, bringing about a lower (hole or electron) current. The voltage dependence of the trap-limited current is an indication of the trap depth, i.e., a stronger voltage dependence implies a deeper trap depth. Due to trap filling, trap-limited conduction shows a steeper voltage dependence than the slope 2 (slope of space-charge-limited current) in a log–log plot.

Using *J*–*V* modeling Nicolai et al. found that electron traps are present in many different polymers and organic small molecules.[78] Independent from the HOMO and LUMO of

© 2023 The Authors. Advanced Materials Technologies published by Wiley-VCH GmbH

2365709x, 2023, 16, Downloaded from https://onlinelibrary.wiley.com/doi/10.1002/admt.202300234 by Technical University Eindhoven, Wiley Online Library on [06/09/2023]. See the Terms and Conditions (https://onlinelibrary.wiley.com/terms-and-conditions) on Wiley Online Library for rules of use; OA articles are governed by the applicable Creative Commons License

organic material the traps are centered at ≈−3.6 eV from the vacuum with a typical distribution width of ≈0.1 eV. Trap densities of ≈1–3 × 10^{17} traps per cm^3 were reported.[78] Further characterization including quantum-chemical studies suggested that water–oxygen complexes cause electron trapping.[78–81] In its neutral state, this complex is only weakly bound. Charge detrapping effectively deactivates the trap. This results in unexpected slow charge trapping rates up to hours.[82] In contrast, Zuo et al. reported a distinct peak in *J–V* curves of single-carrier devices when plotted on a double logarithmic scale.[83] This peak was analyzed in terms of a transition between trap-limited and trap-filled charge transport regimes. Trap depth E_t and trap density N_t were extracted from the height and position of the peak, respectively. Density functional theory (DFT) calculations suggested that water molecules enclosed in nanoscopic voids in the films create both electron and hole traps that lie around 0.3–0.4 eV from the HOMO and LUMO levels, respectively.[83] Finally, Nikolka et al. showed that the presence of water in the polymer film induces a narrow, continuous distribution of hole traps.[84] Incorporation of solvent additives or dopants displaces the water molecules and stable polymer diodes with record SCLC mobilities of up to 0.2 cm^2 V^{-1} s^{-1} were obtained.[84] Molecular doping was also successfully used to make better OPDs.[85–87]

4.2. Charge Recombination Processes in Double-Carrier Devices

Charge transport studies mentioned in Section 4.1 are usually conducted in single carrier diodes. In a double-carrier diode, recombination of electrons and holes should also be taken into account. Parmenter and Ruppel derived an expression for the current density of a double-carrier diode with two Ohmic electrode contacts (excellent injection), for the case of a large applied voltage. With equal and constant electron and hole mobilities, and assuming Langevin recombination, the so-called Parmenter–Ruppel formula reads[88]

$$J \cong 2.88 \frac{9}{8} \varepsilon \mu \frac{V^2}{L^3} \tag{10}$$

The expression for the current density resembles closely the Mott–Gurney law expression for unipolar devices (Equation (4)), albeit that the current density is not just a factor of two larger (as would be expected naively) but a factor of about 2.88. The difference is due to the partially compensating positive and negative space charges in the device. Precisely in the device center, the space charge densities even fully compensate each other. The device is "slightly less space-charge-limited."

For the case of very low bimolecular recombination rates, i.e., a very large Langevin reduction factor γ (see Equation (6)), Equation (10) does no longer hold. In that case both injected carriers can traverse the whole layer, electron and hole densities are approximately equal throughout the whole layer and the current density in this so-called injected plasma limit is given by[89,90]

$$J = \left(\frac{9\pi}{4\gamma} \right)^{1/2} \varepsilon \mu \frac{V^2}{L^3} \tag{11}$$

Martin[91] derived semianalytical solutions for diodes with nonideal contacts and for the case of different electron and hole mobilities. These expressions are however complex and include parameters that have to be determined by a root-finding method.

Measurement techniques to directly quantify the recombination rates and losses are of great significance. Wetzelaer et al. presented an elegant steady-state method to probe bimolecular recombination in organic solar cells at high forward bias.[90] By comparing current densities in a blend in hole-only, electron-only, and double-carrier diodes, charge recombination can be calculated for every voltage and temperature. Results were analyzed in terms of a reduced Langevin recombination factor.

By systematically investigating the change in slope of unipolar current–voltage curves Zuo et al.[92] investigated the effect of adding PCBM on the charge transport properties of polymer donors. Depending on the crystallinity of the polymer, the hole mobility was found to increase or decrease with increasing PCBM content. The decrease in mobility for (semi)crystalline poly(3-hexylthiophene) (P3HT) was attributed to morphological trap formation. The increase in hole mobility in amorphous polymers with PCBM was attributed to the removal of hole traps. The material dependence shows the richness of phenomena and effects that can be found in organic semiconductors, but makes it difficult to make universally applicable claims.

4.3. Diffusion Current and Ideality Factor

From the ideal diode equation (Equation (3)) it can be inferred that the diffusion current depends on the diode ideality factor, n_{id}, and the reverse saturation current, J_0. Both parameters increase with increasing concentrations of trap states. The diode ideality factor is unity in the absence of trap-assisted recombination. The ideality factor is expected to be exactly 2 when recombination takes place predominantly via an immobilized charge in a deep trap state with a free charge, as described by the SRH formalism.[68]

Assuming an exponential band-tail density of states $\exp(E/E_0)$, Van Berkel et al.[93] in 1993 derived an expression of the ideality factor in terms of E_0

$$\frac{1}{n_{id}} = \frac{1}{2} + \frac{kT}{2E_0} \tag{12}$$

It was successfully applied first to amorphous silicon diodes, and later to bulk heterojunction solar cells.[37] It is interesting to note that Equation (12) can explain why the ideality factor can be a noninteger, as measured in amorphous silicon diodes but also in many BHJ devices. De Bruyn et al. provided an alternative explanation for the diffusion current in single-carrier undoped organic diodes with asymmetric contacts in which n_{id} values of ≈1.2 follow from the fact that J_0 becomes dependent on the applied voltage and band bending at the Ohmic contact reduces the built-in voltage.[94] Typical experimental values, however, lie in the range of $1.5 < n_{id} < 1.8$ for double carrier organic photodiodes.[58,95] From the *J–V* characteristics, the ideality factor can be calculated using

$$n_{id} = \left(\frac{kT}{q} \frac{\delta \ln J}{\delta V} \right)^{-1} \tag{13}$$

© 2023 The Authors. Advanced Materials Technologies published by Wiley-VCH GmbH

2365709x, 2023, 16, Downloaded from https://onlinelibrary.wiley.com/doi/10.1002/admt.202300234 by Technical University Eindhoven, Wiley Online Library on [06/09/2023]. See the Terms and Conditions (https://onlinelibrary.wiley.com/terms-and-conditions) on Wiley Online Library for rules of use; OA articles are governed by the applicable Creative Commons License

2365709x, 2023, 16, Downloaded from https://onlinelibrary.wiley.com/doi/10.1002/admt.202300234 by Technical University Eindhoven, Wiley Online Library on [06/09/2023]. See the Terms and Conditions (https://onlinelibrary.wiley.com/terms-and-conditions) on Wiley Online Library for rules of use; OA articles are governed by the applicable Creative Commons License

for voltages where the J–V curve shows a diode behavior and is not limited by shunt series or ambiguous due to hysteretic effects, or by drift current. For PCDTBT:PCBM OPDs we observed n_{id} to be 1.7 (Figure 3). Assuming Equation (12) this corresponds to a E_0 value of 0.14 eV.

4.4. J_0

Temperature-dependent reverse bias dark current measurements can shed light on the origin of the dark current and J_0. Assuming Arrhenius-like temperature behavior, i.e., $J_d \approx J_0 \propto \exp(-E_a/kT)$, where E_a is thermal activation energy of the dark current, E_a can be determined by the slope from $\ln(J_d)$ against reciprocal temperature. In such studies it is of utmost importance that there is no unwanted contribution such as leakage current. Shunt resistance obscures the intrinsic value of J_d and its temperature dependence. Correcting for the shunt resistance is possible, but not ideal. Only if all extrinsic contributions are eliminated, it is possible to derive a meaningful interpretation of J_0.

Ma et al. recently reported in a large set of fullerene and nonfullerene blends in OPDs with ultralow values of J_d (as low as 10^{-9} mA cm^{-2}) that the thermal activation energy barrier of J_d is lower than the effective bandgaps of the blends, by ≈0.3–0.5 eV, but larger than half of the effective bandgap ($E_{e,g}$) of the BHJ.[76] The inset of Figure 4 shows an Arrhenius plot of J_d at −0.1 V and −0.5 V measured for a PCDTBT:PCBM diode from which an activation energy of 0.80–0.92 eV was obtained.[76] Reported $E_{e,g}$ values for PCDTBT:PCBM range from 1.3 eV using photoelectron spectroscopy,[76] to 1.45–1.50 eV using photovoltaic EQE.[96] The thermal activation is thus larger than ½$E_{e,g}$. Also for five other blends the thermal activation energy of J_d is lower than the effective bandgap of the blends, always by ≈0.3–0.5 eV. It was therefore concluded that J_d (in this voltage regime) originates from thermal charge generation involving trap states with depths of ≈0.3–0.5 eV. Very similar results were recently reported by Sandberg et al.[97] Using narrow bandgap BHJ diodes ($E_{e,g}$ < 1.2 eV) they also observe thermally activated reverse-bias dark currents with activation energies that are ≈0.5 eV less than $E_{e,g}$, suggesting in their case trap states at mid bandgap.

The voltage dependence of J_0 at larger negative voltages remains poorly understood. Kublitski et al. suggested that the trap energy depth is lowered by the applied electric field, according to the Poole–Frenkel effect.[21] At larger negative voltages charge injection[5] may start to play a role. Unfortunately, the Poole–Frenkel model as well as the charge injection model both predict J_0 to scale with $F^{1/2}$, where F is the applied electric field.

5. Thermal Admittance Spectroscopy (Capacitance-Based Measurements)

The impedance Z, or equivalently, admittance is measured by applying a small alternating bias voltage of frequency f and measuring the amplitude and phase shift of the resulting current at that frequency. Walter et al. was one of the first to use thermal admittance to characterize the distribution of trap states in thin-film solar cells.[98] It is based on the notion that the maximum frequency at which trapped charges can respond to the applied alternating bias signal (characteristic trap frequency, f_t) is determined by the energy depth of the trap state with respect to the transport energy (E_t). Using the angular frequency $\omega_t = 2\pi f_t$, E_t can be written as

$$\omega_t = 2\nu_0 \exp\left(-\frac{E_t}{kT}\right) \tag{14}$$

with ν_0 the attempt-to-escape frequency.[98] By applying a constant voltage of 0 V or lower, the device is dominantly capacitive and $N(E_t)$ can be expressed as

$$N\left(E_t\right) = -\frac{\omega V_{BI}}{qWkT}\frac{dC\left(\omega\right)}{d\omega} \tag{15}$$

with V_{BI} the built-in voltage, W is the thickness of the active layer, ω is the angular frequency, and $C(\omega)$ is the capacitance. Together with Equation (15), the distribution of the defect states can be determined, provided the attempt-to-escape frequency is known. This parameter can, however, be extracted by temperature-dependent C–f measurements, as the defect distribution is expected to be temperature independent.

To properly evaluate the defect states by admittance spectroscopy the emission of trapped charges must be the slowest step in carrier generation process. For low-mobility BHJ diodes this is not always the case. In BHJ devices with thick active layers and/or at low applied DC voltages, time scales for charge transport are sometimes slower than time scales for trap emission.[99] Interpreting the capacitance response at higher frequencies as coming from a characteristic trap frequency, f_t, leads to an incorrect DOS of trap states.[100]

All this was taken into consideration when Kublitski et al. interpretated their C–f results for optimized small-molecule BHJ OPDs based on 2,2′,6,6′-tetraphenyl-4,4′-bipyranylidene (TPDP) and C_{60} with different donor concentrations (**Figure 5**).[21] The frequency ranges denoted by the hatched areas in Figure 5a were discarded in the trap analyses. With increasing C_{60} concentration, and thus more BHJ interface in the blend, the amount of trap states becomes higher (Figure 5b). Figure 5c illustrates that a higher donor concentration corresponds to a higher trap state density, which is consistent with the trend of higher concentration resulting in higher dark current. By measuring the device under different bias, they proved that the change in the capacitance spectra (10 Hz to 10 kHz) arises from traps instead of energy barriers in the device (Figure 5d). When fitting the trap densities with a Gaussian distribution function N_t, E_t, and the width of the Gaussian, σ, were extracted to be ≈3 × 10^{15} cm^{-3}, 0.5, and 0.04 eV, respectively (Figure 5b). Kublitski et al. also performed temperature dependent J_d measurements on the same diodes. The determined E_a was very close to the energy of trap states measured via impedance spectroscopy.

6. Photoconductivity Measurements

6.1. Light Intensity Dependence of the Open Circuit Voltage

For a diode under illumination, there is no current extraction at open circuit, and the photocurrent balances the injected (dark)

© 2023 The Authors. Advanced Materials Technologies published by Wiley-VCH GmbH

2365709x, 2023, 16, Downloaded from https://onlinelibrary.wiley.com/doi/10.1002/admt.202300234 by Technical University Eindhoven, Wiley Online Library on [06/09/2023]. See the Terms and Conditions (https://onlinelibrary.wiley.com/terms-and-conditions) on Wiley Online Library for rules of use; OA articles are governed by the applicable Creative Commons License

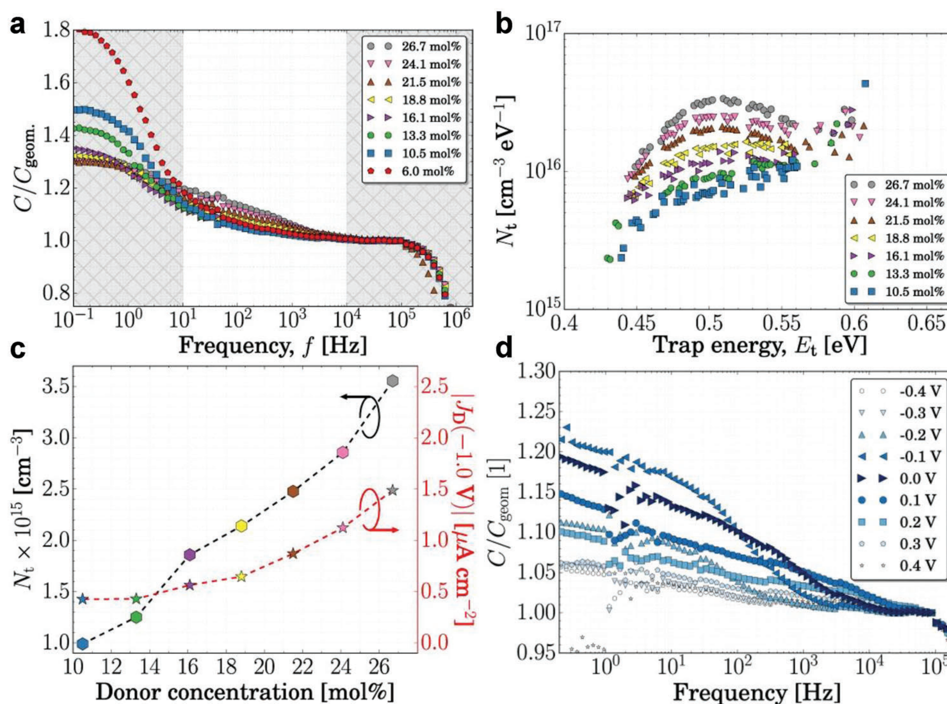

Figure 5. Thermal admittance data of an evaporated OPD using TPDP:C_{60} blends with different D–A mixing ratios: a) Normalized capacitance. Trap states density (N_t) at room temperature. C) Comparison of dark current and trap states density. D) Capacitance spectra at different biases for a device based on TPDP:C_{60} (13.3 mol%). Reproduced with permission Creative Commons CC BY Reproduced under the terms of the Creative Commons Attribution 4.0 International license.[21] Copyright 2021, The Authors, published by Springer Nature.

current. Hence, Equation (2) can be rewritten as

$$V_{oc} = \frac{n_{id}kT}{q} \ln\left(\frac{J_{ph}}{J_0} + 1\right) \tag{16}$$

in which V_{oc} is the open-circuit voltage. Equation (16) predicts that there is a theoretical upper limit for the ratio J_{ph}/J_0 for any given V_{oc}, and that this ratio decreases with decreasing V_{oc}. Gielen et al.[15] plotted V_{oc} versus I_{ph}/I_d on a semilogarithmic scale for a large set of reported BHJs (**Figure 6**). The I_d was collected at –0.1 V to reduce the influence of additional shunt currents. I_{ph} are obtained under high intensity radiation (100 mW cm^{-2}). Series resistances can be neglected at V_{oc}. The red solid line represents the lower thermodynamic limit of the dark current. It can be seen that, with some exceptions, I_{ph}/I_d for most reported BHJ diodes is orders magnitude lower than the intrinsic limit set by the V_{oc}. This is -again- the result of J_d in actual OPDs being much higher than the ideal saturation current, J_0.

Many groups have used light-intensity dependent V_{oc} measurements at relative high-intensity to determine bimolecular recombination rates for solar cells. At low light intensities, trap-assisted recombination may lead to additional voltage losses. With the total amount of trap states being constant, and bimolecular recombination becoming quadratically stronger, n_{id} decreases with increasing light intensity, and a crossover from a trap-assisted to a bimolecular recombination dominated regime is anticipated. First predicted by Mandoc,[101] this crossover was experimentally reported by several groups.[102–104]

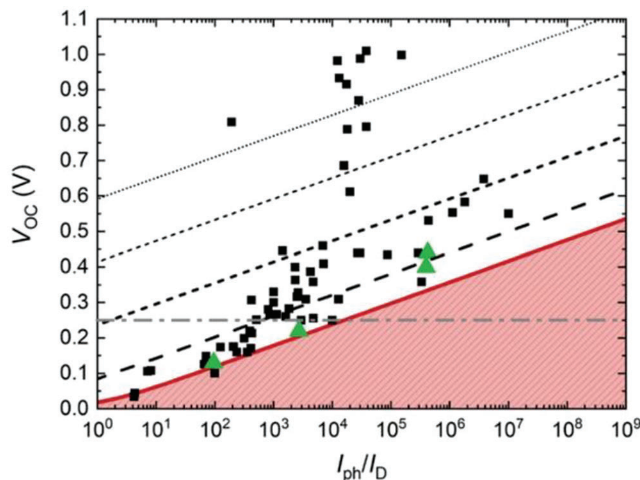

Figure 6. Open-circuit voltage, V_{oc}, versus current ratio of photocurrent to dark current, I_{ph}/I_d, for a large set of organic BHJ device. Reproduced under the terms of the Creative Commons Attribution 4.0 International license.[15] Copyright 2020, Wiley–VCH GmbH.

From temperature-dependent V_{oc} measurements in polymer diodes with trap-limited electron currents. Kuik et al. observed that the activation energy of the trap-assisted recombination process equals that of the hole mobility.[69] They concluded that the rate limiting step for this mechanism is the diffusion of free holes toward trapped electrons, linking Langevin and

© 2023 The Authors. Advanced Materials Technologies published by Wiley-VCH GmbH

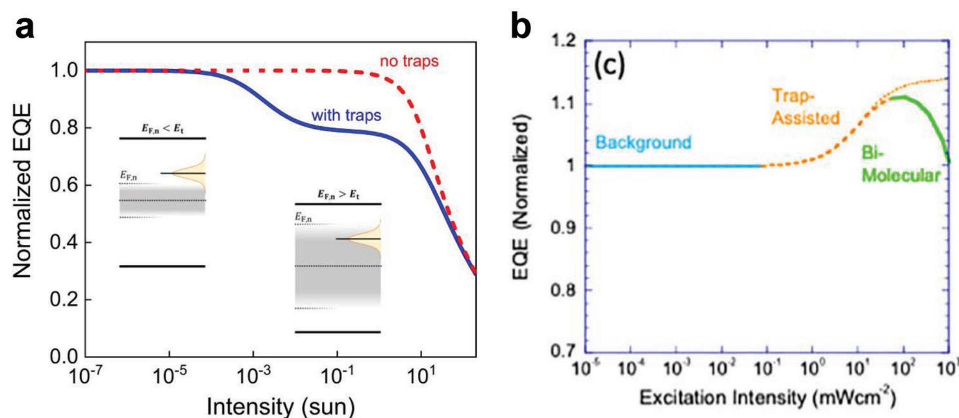

Figure 7. Normalized EQE as a function of light intensity. A) With increase in light intensity and quasi-Fermi level splitting, certain trap states become filled with photogenerated charges, resulting in an increase of trap-assisted charge recombination. B) With increase in light intensity, trapped "dark" charges near the contact are emptied due to recombination with photo carriers, effectively decreasing trap-assisted recombination strength with light intensity. At even higher light intensities (>10 mW cm^{-2}) bimolecular recombination becomes dominant. Reproduced under the terms of the Creative Commons Attribution 4.0 International license.[105] Copyright 2021, The Authors, published by Springer Nature. Reproduced with permission.[108] Copyright 2022, American Institute of Physics.

SRH recombination in an elegant way. This correlation can also be made mathematically: At high light intensities, when $n_e n_h >> n_i^2$, and $n_e \approx n_h$, and then when also $C_p << C_n$ applies, the SRH recombination rate in Equation (7) simplifies to $R_{SRH} = C_p N_t n_h$. The estimated room temperature capture coefficient of $\approx 1 \times 10^{-18}$ m^3 s^{-1} was in close agreement with capture values reported for organic solar cells.[75,101] Furthermore, for a wide temperature range it was found that $C_p(T) = q\mu(T)/\epsilon$. This relationship follows from the Langevin recombination rate (Equation (5)) for an immobilized electron, i.e., $\mu_e = 0$.

6.2. Light Intensity-Dependent Short-Circuit Current Measurements

Light intensity-dependent photocurrent measurements have been widely used to characterize the photocurrent losses under operational condition, typically at short circuit.[62,105] At short circuit, the internal field V_{BI} is high and in state-of-the-art BHJ almost all photogenerated charge carriers are efficiently collected at the contacts. In the absence of significant recombination, no absorption losses and 100% charge carrier generation, the short-circuit current density (J_{sc}) is given by $J_{sc} = \gamma q P$ with P the photon flux of the incident light, and γ a proportionality factor that accounts for the efficiency by which the light is absorbed and charges are created by the BHJ blend and subsequently collected at the contacts. As every device suffers from optical and charge generation losses, EQEs are therefore less than 100%. At high photon flux, the buildup of space charge inside the active layer (due to an imbalance of electron and hole mobilities),[106,107] or bimolecular recombination can also result in lower collection efficiency, resulting in $J_{sc} \propto P^\alpha$, with α being smaller than 1, respectively. At lower light intensities, these effects are negligible. We note that first-order recombination losses do not easily manifest themselves as a nonlinear light-intensity dependence of J_{sc}, but simply result in a lower EQE value. It is therefore remarkable that in very recent reports the photocurrent in OPDs increased both sublinearly[105] and superlinearly[108–110] with light intensity at low light intensities. In both cases, the nonlinear behavior was ascribed to the presence of trap states.[105,108,110,111] The proposed mechanisms are shown in **Figure 7**.

Zeiske et al.[105] explained the sublinear dependence of the photoconductivity on light intensity in terms of an increase in the number of recombination centers due to widening of the quasi-Fermi levels in combination with off-centered trap states. At low light intensities, the photocurrent loss is independent on intensity. Under moderate light intensities with higher carrier density, the quasi-Fermi level crosses the energy level of sub-bandgap states, converting them from traps to recombination centers. The trap-assisted (SRH) recombination increases, resulting in a loss in photocurrent: a second plateau in EQE with lower magnitude is observed. At even higher intensity, second-order bimolecular recombination starts to play a role and further reduces the EQE with increasing light intensity.

The trap-assisted recombination rate depends on the density of recombination centers (and thus light intensity), and its onset is quantified by the position of the quasi-Fermi level $E_{f,n}$ ($E_{f,p}$) for free electrons (holes) relative to the trap energy E_t. Since the SRH recombination is expected to rise and saturate at the trap-filling limit, there is a point-of-transition (POT) between the low intensity regime, where first-order SRH recombination is negligible, and the moderate intensity regime where it dominates (trap-filling limit). Thus, this intensity onset (POT) for the first-order SRH recombination shown in the EQE versus light intensity can be used to determine the trap depth. For electron traps, the critical electron density at which $E_{f,n}$ equals E_t (POT) can be used to determine the trap energy via

$$n_1 = N_{L,A} \exp\left(-\frac{\Delta_t}{kT}\right) \tag{17}$$

where $N_{L,A}$ is the density of transport states in the LUMO of the acceptor and Δ_t is the energy difference between

© 2023 The Authors. Advanced Materials Technologies published by Wiley-VCH GmbH

2365709x, 2023, 16, Downloaded from https://onlinelibrary.wiley.com/doi/10.1002/admt.202300234 by Technical University Eindhoven, Wiley Online Library on [06/09/2023]. See the Terms and Conditions (https://onlinelibrary.wiley.com/terms-and-conditions) on Wiley Online Library for rules of use; OA articles are governed by the applicable Creative Commons License

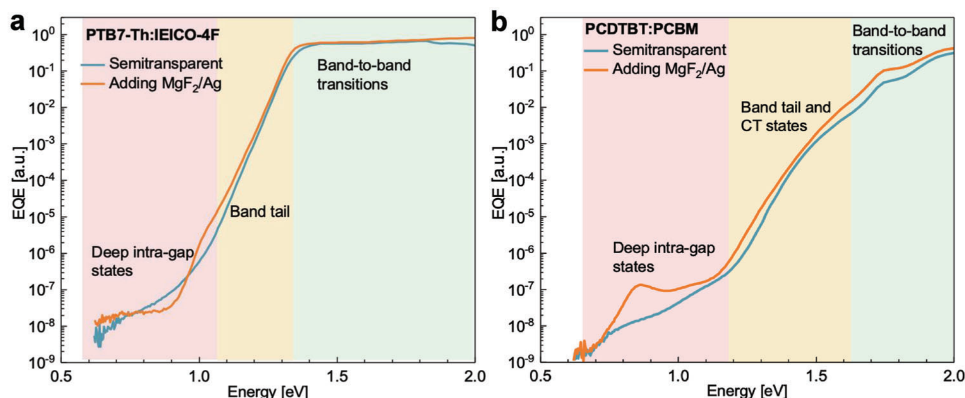

Figure 8. a) EQE spectra of a PTB7-Th:IEICO-4F diode with a semitransparent stack (ITO/ZnO/BHJ/MoO_3/ITO) and the same OPD device with a MgF_2 optical spacer and Ag mirror on top of the ITO back electrode. b) Same for PCDTBT:PCBM. The blue lines are the spectra of the semitransparent devices, the orange lines are spectra of same devices with the MgF_2/Ag layers on top. Reproduced under the terms of the Creative Commons Attribution 4.0 International license.[76] Copyright 2022, The Authors, published by Wiley–VCH GmbH.

sub-bandgap states and LUMO of acceptor. By this method, Zeiske et al.[105] concluded that the photocurrent losses are due to energy states lying 0.35–0.6 eV below the transport edge for a wide variety of organic semiconductors. The EQE losses are small, only 3–10%, and determined by a few data points which leads to considerable uncertainty of ±0.1 eV for the trap depth.[105]

Liraz et al.[108] showed that in their OPDs the light intensity dependent EQE curve at 0 V and forward bias (with extra contact injection) is different from that observed by Zeiske et al. Here, the EQE first increases with light intensity before it decreases due to bimolecular recombination. The counterintuitive EQE enhancement at low light intensity was explained by the role of trapped "dark" charges near the contact. In dark, there is an excess of charges that have diffused from the contact into the semiconductor (see Section 3) and the trap states are almost completely full. At low light intensities, these "dark" trapped charges recombine with photogenerated carriers, reducing trap occupation. This is referred to as trap emptying (Figure 7b). With further increase in light intensity the density of the photocarriers becomes much larger than the density of trapped charges ($n \sim p >> N_t$), and the occupation ratio becomes equal to 50%, effectively resulting in a loss in trap-assisted recombination rate, which explains the net increase in EQE. The trap emptying mechanism can take place only when part of the traps in dark are occupied because the trap states located close to the center of the gap (Fermi level is located within defect band) or by injection current (quasi-Fermi level is located within defect band).

This effect was modeled in more detail by Hartnagel and Kirchartz.[111] Using numerical drift-diffusion modeling the nonlinearity at low light intensity was found to result from light-dependent pseudofirst order losses between injected, trapped dark carriers near the contacts and photogenerated carriers.[111] The density of trapped carriers decreases (or increases sublinearly) with increasing light intensity. This leads to a reduced recombination rate with light intensity since the total trap-induced recombination scales with $n_e\, p_t + n_h\, n_t$, where p_t and n_t denote the trap densities near the contacts. The net result is a superlinear photocurrent behavior at low light intensity.

6.3. Sub-Bandgap External Quantum Efficiency (EQE) Measurements

The density of localized trap states is typically four to six orders of magnitude lower than that of states above the transport energy.[112,113] Determining the energetic distribution of the trap states is rather difficult and has remained a challenge. Recently, ultrasensitive photocurrent measurements with a detection limit of ≈fA that allow determining external quantum efficiencies (EQE) down to 10^{-9}, have been applied to investigate intra-bandgap states in organic photodiodes.[114–116]

Due to disorder, organic semiconductors absorb light at photon energies below the bandgap (sub-bandgap absorption). Just below the band edge EQE usually decreases exponentially with decreasing photon energy. The steepness of this exponential tail is related to the Urbach energy, a parameter that is often associated with the energetic disorder of the BHJ.[117,118] **Figure 8**a shows the ultrasensitive EQE spectrum of a PTB7-Th:IEICO-4F photodiode (in which PTB7-Th is poly[[4,8-bis[5-(2-ethylhexyl)-2-thienyl]benzo[1,2-*b*:4,5-*b*′]dithiophene-2,6-diyl]-alt-[2-[[(2-ethylhexyl)oxy]carbonyl]-3-fluorothieno[3,4-*b*]thiophenediyl]] and IEICO-4F is 2,2′-((2Z,2′Z)-(((4,4,9,9-tetrakis(4-hexylphenyl)-4,9-dihydro-s-indaceno[1,2-*b*:5,6-*b*′]dithiophene-2,7-diyl)bis(4-((2-ethylhexyl)oxy)thiophene-5,2-diyl))bis(methaneylylidene))bis(5,6-difluoro-3-oxo-2,3-dihydro-1*H*-indene-2,1-diylidene))dimalononitrile). The spectrum shows the exponential tail with an energy of 29 meV fitting by Urbach's rule.[117] Figure 8b shows a similar EQE spectrum of PCDTBT:PCBM. In this case, the exponential Urbach tail is not visible. Instead, a broad Gaussian line shape can be seen which is caused by an absorption band centered at an energy of around 1.4 eV and ascribed to a charge transfer (CT) transition from the donor to the acceptor with an energy E_{CT}. Similar spectral features were reported by others for PCDTBT:PCBM diodes.[50,114] The presence of a CT state makes it impossible to extract an Urbach energy for this layer. Below the CT band, distinct low-energy EQE signals are present. These low-energy bands were found in a wide range of D–A combinations and associated with the absorption of low-energy photons and indicate the

© 2023 The Authors. Advanced Materials Technologies published by Wiley-VCH GmbH

2365709x, 2023, 16, Downloaded from https://onlinelibrary.wiley.com/doi/10.1002/admt.202300234 by Technical University Eindhoven, Wiley Online Library on [06/09/2023]. See the Terms and Conditions (https://onlinelibrary.wiley.com/terms-and-conditions) on Wiley Online Library for rules of use; OA articles are governed by the applicable Creative Commons License

presence of intra-bandgap states. The low-energy onsets of these low-energy bands represent the lowest-energy photoexcitations that can generate photocurrent in the OPDs and coincides nicely with the activation energy of J_d of 0.8–0.9 eV (see Section 4.3).[76]

The radiative dark saturation current density can be calculated by integrating the product of the EQE(E) and the temperature dependent black body spectrum via Equation (18)

$$J_0^{\mathrm{R}}(T) = q\int_{E_{\min}}^{\infty} \mathrm{EQE}(E)\Phi_{\mathrm{BB}}(T,E)dE \tag{18}$$

with $\Phi_{\mathrm{BB}}(T,E)$ the black body spectrum at temperature T. The lower integration limit $E_{\min}$ is ideally zero but in practice given by the lower limit of the sub-bandgap EQE measurement or extrapolated to lower energies with a hypothetic distribution of intra-bandgap states.[119] Considering that $\Phi_{\mathrm{BB}}(T,E)$ increases exponentially with decreasing photon energy E, the integration of $\mathrm{EQE}(E)\Phi_{\mathrm{BB}}(T,E)$ largely depends on the absorption features at sub-bandgap region. The dark saturation current density (J_0) of an OPD consists of $J_0^{\mathrm{R}}(T)$and a nonradiative contribution (J_0^{NR}), and can be estimated from

$$J_0 = J_0^{\mathrm{R}}/\mathrm{EQE}_{\mathrm{EL}} \tag{19}$$

with $\mathrm{EQE}_{\mathrm{EL}}$ the electroluminescence quantum efficiency. Values of 10^{-5}–10^{-7} are typical for organic BHJs.[15,29,114,120,121] This supports the idea that J_d consists of small radiative and large nonradiative dark saturation current densities, where the radiative part is thermally generated via intra-bandgap states. Assuming that EQE(E) and $\mathrm{EQE}_{\mathrm{EL}}(E)$ are temperature independent, J_0 at different temperatures can be calculated via Equations (18) and (19) using the black body radiation at different temperatures. In such case it is in principle possible to estimate the activation energy (E_a) of J_0 by plotting the $J_0^{\mathrm{R}}(T)$versus $1/kT$ and fit the data to an Arrhenius equation.

To determine the energetic distribution of the intra-bandgap states, the EQE spectra in the sub-bandgap region have been fitted to a Marcus model,[114] representing a transition between two localized states with vibrational progression, and to a model based on a transition between a trap with a Gaussian-distributed energy to the valence or conduction band.[122–125] Both models describe the onset, but the latter better reproduces the plateau in sub-bandgap region. We note, however, that the sub-bandgap EQE spectra are strongly affected by interference.

This became evident by adding an optical spacer-mirror to semitransparent perovskite detectors.[124] Adding such as optical spacer to PCDTBT:PCBM OPD strongly influences the sub-bandgap signal in the EQE spectra. Instead of a gradual increase, a distinct onset followed by a plateau is found (compare two spectra in Figure 8b): a modulating interference pattern appears in the EQE spectrum, indicating strong variations of the optical electric field. The interference peak at 0.85 eV clearly shows that the EQE spectra in sub-bandgap region can change drastically due to optical interference, and that fitting the EQE spectra to obtain information on the energy of intra-bandgap states without considering the cavity effect is questionable.

6.4. Transient Photocurrent Measurements

Figure 9a shows schematically the time scales associated with photo-induced charge carrier generation, dissociation, detrapping, and extraction. The photoresponse time, or operation bandwidth, of a PD corresponds to the time required to generate and extract the photocarriers. The 1–10 ms time response found in organic photodiodes is relatively slow compared to inorganic counterparts due to the low charge carrier mobility of organic semiconductors.[126–128] The carrier transit time τ_{tr} is determined by

$$\tau_{\mathrm{tr}} = \frac{L^2}{2\mu\left(V - V_{\mathrm{BI}}\right)} \tag{20}$$

The factor of 2 in Equation (20) accounts for the fact that, on average, mobile carriers must travel through only approximately half the film thickness. Equation (20) is only approximate; it does not take into account that a distribution of mobility values is expected in disordered semiconductors. Using $\mu \approx 10^{-4}$ cm^2 V^{-1} s^{-1}, $L \approx 300$ nm, and V–$V_{\mathrm{BI}} \approx 0.5$ V, a carrier transit time of 10^{-5} s is obtained.

The cut-off frequency ($f_{-3\mathrm{dB}}$) is also used to characterize the dynamic behavior of OPDs. It is defined as the modulation frequency of input light at which the measured photoresponse is −3 dB lower than the response under continuous illumination. This means that at the cut-off frequency, the measured current J_{ph} decreased to $1/\sqrt{2}$ of its initial value at the lowest frequency. $f_{-3\mathrm{dB}}$ depends on the carrier transit time (τ_{tr}) and the RC-time, which is the product of resistance (R) and capacitance (C), of the equivalent circuit, and can be estimated from[129,130]

$$\frac{1}{f_{-3\,\mathrm{dB}}^2} = \frac{1}{f_{\mathrm{tr}}^2} + \frac{1}{f_{\mathrm{RC}}^2} = \left(\frac{2\pi\tau_{\mathrm{tr}}}{3.5}\right)^2 + (2\pi RC)^2 \tag{21}$$

In case the response speed is RC limited, reducing the device effective area and series resistance will improve $f_{-3\mathrm{dB}}$.[20,131,132] The presence of trap states will degrade the photoresponse time.[44,133–140] The extraction dynamics are primarily determined by the time it takes before a trapped charge is thermally released. Charge (de)trapping effects are more prominent at low light intensities. At sufficiently high light intensities, the number of generated carriers is so large that all trap states are filled. At even higher high light intensity, other factors can become important (such as built-up of a space-charge).

Arca et al.[133] found that $f_{-3\mathrm{dB}}$ of polymer:PCBM photodetector at very low light intensity (<200 nW cm^{-2}) was two orders of magnitude lower than at high light intensity. By changing the material of the hole transport layer (HTL) the light intensity dependence of the cut-off frequency was largely eliminated, indicating that traps at the interface between the BHJ and anode were responsible for lowering the response speed. In a series of papers, McNeil and co-workers studied the photoresponse to a square pulse of light, varying the light intensity and applied voltage.[135,136,141] A fast rise of ≈1 ms followed by a slow rise of order 10–100 ms was typically found, as well as a fast microsecond decay component after turn-off with a small, long-lived tail that persists up to milliseconds. The fast rise and decay are attributed to the transport of mobile carriers, whereas the slow rise and decay components

© 2023 The Authors. Advanced Materials Technologies published by Wiley-VCH GmbH

2365709x, 2023, 16, Downloaded from https://onlinelibrary.wiley.com/doi/10.1002/admt.202300234 by Technical University Eindhoven, Wiley Online Library on [06/09/2023]. See the Terms and Conditions (https://onlinelibrary.wiley.com/terms-and-conditions) on Wiley Online Library for rules of use; OA articles are governed by the applicable Creative Commons License

2365709x, 2023, 16, Downloaded from https://onlinelibrary.wiley.com/doi/10.1002/admt.202300234 by Technical University Eindhoven, Wiley Online Library on [06/09/2023]. See the Terms and Conditions (https://onlinelibrary.wiley.com/terms-and-conditions) on Wiley Online Library for rules of use; OA articles are governed by the applicable Creative Commons License

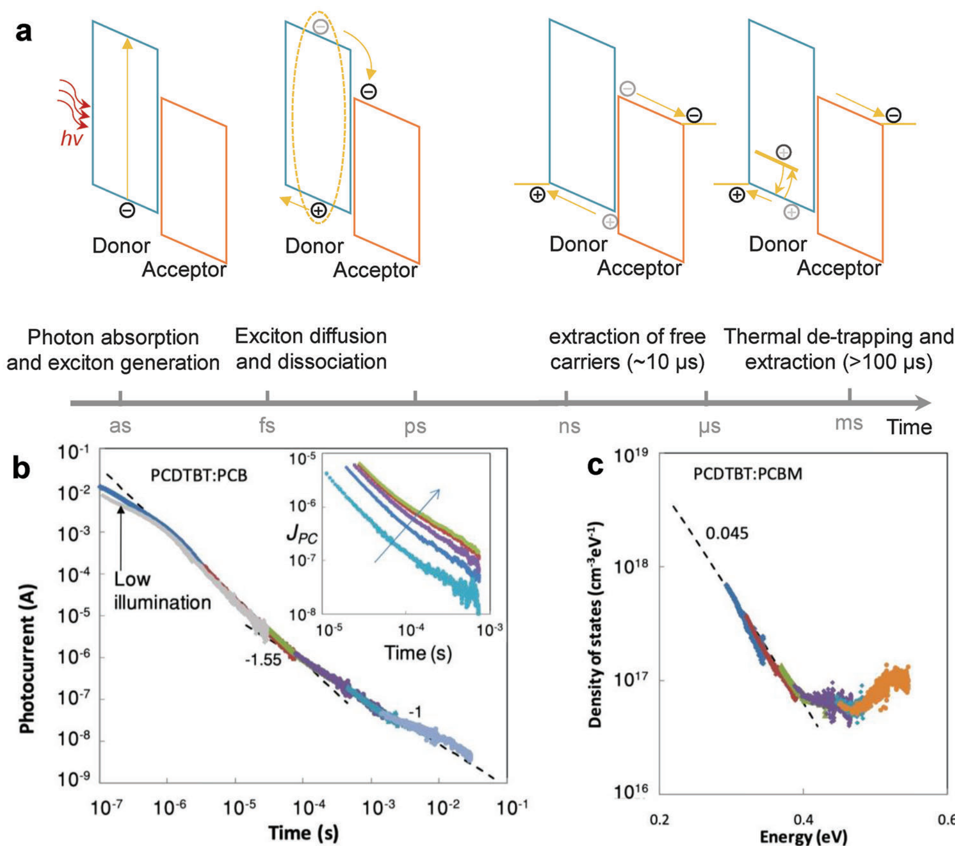

Figure 9. a) Physical processes of photo-induced charge carrier generation, dissociation, detrapping, and extraction, plus their associated time scales. For clarity, light absorption, and charge trapping are shown in the donor material only. b) A group of transient photocurrent measurements of PCDTBT:PCBM measured at times extending beyond the transit time, indicated by different colors, spanning in total six orders of magnitude in time. Inset plot shows the transients with increasing illumination intensity. c) Extracted DOS distribution for PCDTBT:PCBM from (b). The dashed line is an exponential with the indicated slope parameter E_0. Reproduced with permission.[142] Copyright 2011, American Physical Society.

are explained by charge trapping and detrapping processes.[136] Numerical simulations using a single trap level ($N_t = 1.3 \times 10^{16}$ cm^{-3}, $E_t = 80$ meV) was used to reproduce the measured photocurrent transients, including the photocurrent tail characteristic long persistent current tail[136] with magnitude that does not scale linearly with light intensity or steady-state photocurrent. From the long photocurrent tail, the trap distribution $N(E)$ can be deduced in case the measured photocurrent at measurement time t is due to thermal detrapping of charges at a trap depth equal to the demarcation energy $E_D(t)$. It implicitly assumes that there is no recombination (because only one type of charge carrier is trapped, i.e., charge carriers of the opposite sign are fully extracted and charge injection currents are negligibly small) and the thermally excited trap is not trapped again but extracted at the contact. The $E_D(t)$ is given by the equation

$$E_D(t) = kT \ln(\omega_0 t) \tag{22}$$

where ω_0 is an attempt-to-escape prefactor (see also Section 5). The persistent photocurrent $J_{PC}(t)$ is given by

$$J_{PC}(t) = qALfN(E_D)\frac{dE_D}{dt} \tag{23}$$

where A is active area of the device, L its thickness, f is the fraction of states filled (usually taken to be 100%), and $N(E_D)$ is trap density at energy of E_D.

Street deduced the DOS of band tail $N(E)$ from transient current $J_{PC}(t)$ for polymer:PCBM diodes by plotted the product of the photocurrent and the measurement time (Figure 9b) against the demarcation energy.[142] For PCDTBT:PCBM, the calculated DOS decreases from $\approx 10^{18}$ to $\approx 10^{17}$cm^{-3} eV^{-1} between the energy depth of 0.3–0.4 eV with a slope of $E_0 \approx 45$ meV (Figure 9c). The structure near 0.42 and 0.53 eV might reflect discrete levels. For P3HT:PCBM, a transition of exponential slope was observed changing from 45 to 65 meV at trap energy of 0.35 eV, suggesting a different degree of disorder or perhaps broad distribution of impurities.

Although this is conceptually a simple method to characterize the states in the bandgap, it involves some assumptions and uncertainty. MacKenzie et al. systematically investigated the conditions under which the transient current measurements can retain a faithful image of the density of states.[138] Key assumption is the absence of recombination, see above. The energy scale is determined by the attempt-to-escape prefactor, ω_0, relating to magnitude of the capture cross section. The ω_0 is assumed to be 10^{11} –10^{12} s^{-1} in these studies but not directly measured.[142] An

© 2023 The Authors. Advanced Materials Technologies published by Wiley-VCH GmbH

order of magnitude changes in ω_0 corresponding to a shift of 0.06 eV in the energy scale.

7. Outlook and Recommendations

This work reviews the concepts involved in dark and photoconductivity in organic BHJ diodes. There is substantial agreement that intra-bandgap states play an important role in many aspects relevant for their application as photodetector. We have seen that intra-bandgap electronic states increase dark current and dark noise, effectively decreasing the specific detectivity. Moreover, charge trapping and recombination result in nonlinear photoresponse at low light intensities. Finally, slow thermal release of trapped carriers results in a slow persistent photocurrent that causes image lag. Much more work must be done in this field to determine unambiguously the microscopic origin of the most important defect states, and their electronic characteristics with the final aim to mitigate their detrimental effects. In the meantime, it is important to relate these states to important detector metrics such as D^*, dark current, responsivity, and response time. All this requires careful device studies, which leads us to the following recommendations:

7.1. Recommendations for Dark Current Studies

Understanding the factors that determine i_n and J_d is an important prerequisite to further reduce the J_d and thereby improve D^*.

It is crucial that the OPD must have a small leakage current density and therefore a high shunt resistance. It is important to make sure there is no other extra unwanted contribution such as lateral leakage current or injection current. Lateral leakage can be successfully suppressed by the edge cover layer (ECL)—made of an insulating dielectric—without compromising the photocurrent response.[76,143,144]

At low dark currents, displacement currents are non-negligible, even at very low scan rates. These effects are evidenced by nonzero J_d at 0 V and hysteretic effects in the low current voltage range. We advise measurements under constant bias for more accurate measurements.

At larger reverse bias, injection current from the contact can also contribute to the dark current. Thus, to investigate trap-assisted thermal charge generation, the reverse bias should be as small as possible, but trap-induced charge injection lowering seems to be a distinct possibility now that OPDs can be produced with a low density of deep energy states in the bulk. Systematic bias and temperature dependent dark current measurements are likely to separate charge injection from thermal charge generation.

Also in this work, the analytical discussion is mostly centered on steady-state dark current, even though it is clear that OPDs are not shot noise limited.[3,4,10,15,21,24,26,86,87,109,110,131,146–170] Noise current measurements are strongly recommended when calculating specific detectivity values. Moreover, frequency-dependent noise current measurements can shed light on the energy distribution of traps and recombination states, in dark and in light.

7.2. Recommendations for Photocurrent Studies

Particularly at low light intensities it becomes again important that OPDs have a high shunt resistance. The light intensity dependent short circuit photocurrent technique is an important tool for probing details of the recombination.

Special caution should be taken in low light intensity regime where the photocurrent is comparable to the reverse dark current. This thermal activated dark current can be mistakenly perceived as photocurrent at the short-circuit condition and cause the underestimate of photocurrent loss. Using modulated light source and measuring the short circuit current with a certain frequency via lock-in amplifier can eliminate the contribution of dark current.[105,108,145]

Hartnagel and Kirchartz[111] convincingly demonstrated the short comings of a 0D model to explain light-dependent photocurrent behavior. In OPDs charge recombination rates at low light intensities are strongly dependent on the background "dark" carriers close to the electrode. A direct connection between trap distribution and OPD performance can be established using numerical drift-diffusion modeling.

Much more work must be done in this area to determine unambiguously the trapping parameters of the dominant defects but also the exact mechanism of recombination. SRH recombination is used by default in many software programs and may be appropriate but—by definition—always has a strong propensity to midgap states. It may be more appropriate to describe recombination in organic BHJ diodes in terms of the detailed diffusion of the electron and hole to each other to accomplish a recombination event at the donor–acceptor interface.

Sub-bandgap EQE measurements provide a powerful new way to investigate sub-bandgap states in organic devices. It would be useful to establish a framework to estimate the trap distribution from such spectra, taking into consideration the presence of possible interference effects.

Subtle nonlinearities of the light dependence of J_{ph} as a function of light intensity are better visible when plotting the responsivity (or EQE) as a function of light intensity instead of the often seen log–log plot of J_{ph} versus light intensity. Nonlinearities are expected at both high and low light intensities, and are important when extracting the linear dynamic range (LDR) of the photodetector. At low light intensities, the deviation from the linearity of photocurrent is fundamentally related to a change in trap occupation with light intensity. At high light intensities, bimolecular (Langevin) recombination will become dominant, and result in a $J_{ph} \propto P^{\alpha}$ with α lower than unity.

Strictly speaking, the linear dynamic range (LDR) indicates the light intensity range in which the photoresponse is linearly dependent on incident light intensity, i.e., $J_{ph} \propto P^{\alpha}$ with $\alpha = 1.00$. It implies that—within this range—the processes of charge carrier generation and recombination are independent of the light intensity, which is translated to a constant responsivity. When determining LDR, J_{min} and J_{max} represent the minimum and maximum value of linearly responded photocurrent density, respectively. As discussed by Kielar et al.[131] ambiguity exists how to determine J_{min} and J_{max}. Linearity, or more correctly, nonlinearity, is a measure of the maximum deviation of the photocurrent from a specified straight line. There is no absolute criterion of the linearity error that can be tolerated. L_{min} is affected by the

© 2023 The Authors. Advanced Materials Technologies published by Wiley-VCH GmbH
2365709x, 2023, 16, Downloaded from https://onlinelibrary.wiley.com/doi/10.1002/admt.202300234 by Technical University Eindhoven, Wiley Online Library on [06/09/2023]. See the Terms and Conditions (https://onlinelibrary.wiley.com/terms-and-conditions) on Wiley Online Library for rules of use; OA articles are governed by the applicable Creative Commons License

2365709x, 2023, 16, Downloaded from https://onlinelibrary.wiley.com/doi/10.1002/admt.202300234 by Technical University Eindhoven, Wiley Online Library on [06/09/2023]. See the Terms and Conditions (https://onlinelibrary.wiley.com/terms-and-conditions) on Wiley Online Library for rules of use; OA articles are governed by the applicable Creative Commons License

trap density as well as the trap depth. L_{max} is related to bimolecular (Langevin) recombination, and thus determined by the ratio between the slower carrier mobility μ and the (Langevin) reduction factor γ (Equation (6)), J_{max} thus can theoretically be pushed to higher values by using low-mobility donor and acceptor materials, and combinations thereof which show a high reduced Langevin recombination rate.

Supporting Information

Supporting Information is available from the Wiley Online Library or from the author.

Acknowledgements

The authors acknowledged funding from the Ministry of Education, Culture, and Science (Gravity program 024.001.035) and from Netherlands Organisation for Scientific Research (NWO Spinoza grant).

Conflict of Interest

The authors declare no conflict of interest.

Keywords

bulk heterojunctions, charge recombination, organic photodetectors, trap states

Received: February 15, 2023
Revised: May 12, 2023
Published online: June 19, 2023

[1] T. N. Ng, W. S. Wong, M. L. Chabinyc, S. Sambandan, R. A. Street, *Appl. Phys. Lett.* **2008**, *92*, 213303.
[2] T. Someya, S. Iba, Y. Kato, T. Sekitani, Y. Noguchi, Y. Murase, H. Kawaguchi, T. Sakurai, in *Electron Devices Meeting, IEDM Technical Digest (IEEE International)*, IEEE, NJ **2004**, p. 365.
[3] G. H. Gelinck, A. Kumar, D. Moet, J. L. P. J. v d Steen, A. J. J. M. v Breemen, S. Shanmugam, A. Langen, J. Gilot, P. Groen, R. Andriessen, M. Simon, W. Ruetten, A. U. Douglas, R. Raaijmakers, P. E. Malinowski, K. Myny, *IEEE Trans. Electron Devices* **2016**, *63*, 197.
[4] A. J. J. M. van Breemen, M. Simon, O. Tousignant, S. Shanmugam, J.-L. van der Steen, H. B. Akkerman, A. Kronemeijer, W. Ruetten, R. Raaijmakers, L. Alving, J. Jacobs, P. E. Malinowski, F. De Roose, G. H. Gelinck, *Npj Flex Electron.* **2020**, *4*, 22.
[5] G. Simone, D. Di Carlo Rasi, X. de Vries, G. H. L. Heintges, S. C. J. Meskers, R. A. J. Janssen, G. H. Gelinck, *Adv. Mater.* **2018**, *30*, 1804678.
[6] D. Tordera, B. Peeters, H. B. Akkerman, A. J. J. M. van Breemen, J. Maas, S. Shanmugam, A. J. Kronemeijer, G. H. Gelinck, *Adv. Mater. Technol.* **2019**, *4*, 1900651.
[7] H. Akkerman, B. Peeters, A. Van Breemen, S. Shanmugam, D. Tordera, J.-L. van der Steen, A. J. Kronemeijer, P. E. Malinowski, F. De Roose, D. Cheyns, J. Genoe, W. Dehaene, P. Heremans, G. Gelinck, *SID Sym. Dig. Tech. Pap.* **2018**, *49*, 494.
[8] Y. Wei, H. Chen, T. Liu, S. Wang, Y. Jiang, Y. Song, J. Zhang, X. Zhang, G. Lu, F. Huang, Z. Wei, H. Huang, *Adv. Funct. Mater.* **2021**, *31*, 2106326.
[9] M. Babics, H. Bristow, W. Zhang, A. Wadsworth, M. Neophytou, N. Gasparini, I. McCulloch, *J. Mater. Chem. C* **2021**, *9*, 2375.
[10] M. Biele, C. Montenegro Benavides, J. Hürdler, S. F. Tedde, C. J. Brabec, O. Schmidt, *Adv. Mater. Technol.* **2019**, *4*, 1800158.
[11] K. H. Hendriks, W. Li, M. M. Wienk, R. A. J. Janssen, *J. Am. Chem. Soc.* **2014**, *136*, 12130.
[12] N. Gasparini, A. Gregori, M. Salvador, M. Biele, A. Wadsworth, S. Tedde, D. Baran, I. McCulloch, C. J. Brabec, *Adv. Mater. Technol.* **2018**, *3*, 1800104.
[13] Y.-J. Cheng, S.-H. Yang, C.-S. Hsu, *Chem. Rev.* **2009**, *109*, 5868.
[14] L. Dou, Y. Liu, Z. Hong, G. Li, Y. Yang, *Chem. Rev.* **2015**, *115*, 12633.
[15] S. Gielen, C. Kaiser, F. Verstraeten, J. Kublitski, J. Benduhn, D. Spoltore, P. Verstappen, W. Maes, P. Meredith, A. Armin, K. Vandewal, *Adv. Mater.* **2020**, *32*, 2003818.
[16] Q. Li, Y. Guo, Y. Liu, *Chem. Mater.* **2019**, *31*, 6359.
[17] A. Wadsworth, Z. Hamid, J. Kosco, N. Gasparini, I. McCulloch, *Adv. Mater.* **2020**, *32*, 2001763.
[18] J. Lee, S.-J. Ko, M. Seifrid, H. Lee, B. R. Luginbuhl, A. Karki, M. Ford, K. Rosenthal, K. Cho, T.-Q. Nguyen, G. C. Bazan, *Adv. Energy Mater.* **2018**, *8*, 1801212.
[19] H. Yao, Y. Cui, R. Yu, B. Gao, H. Zhang, J. Hou, *Angew. Chem., Int. Ed.* **2017**, *56*, 3045.
[20] F. P. García De Arquer, A. Armin, P. Meredith, E. H. Sargent, *Nat. Rev. Mater.* **2017**, *2*, 16100.
[21] J. Kublitski, A. Hofacker, B. K. Boroujeni, J. Benduhn, V. C. Nikolis, C. Kaiser, D. Spoltore, H. Kleemann, A. Fischer, F. Ellinger, K. Vandewal, K. Leo, *Nat. Commun.* **2021**, *12*, 551.
[22] Y. Fang, A. Armin, P. Meredith, J. Huang, *Nat. Photonics* **2019**, *13*, 1.
[23] I. K. Kim, J. H. Jo, J. Lee, Y. J. Choi, *Org. Electron.* **2018**, *57*, 89.
[24] Z. Wu, W. Yao, A. E. London, J. D. Azoulay, T. N. Ng, *Adv. Funct. Mater.* **2018**, *28*, 1800391.
[25] T. Li, G. Hu, L. Tao, J. Jiang, J. Xin, Y. Li, W. Ma, L. Shen, Y. Fang, Y. Lin, *Sci. Adv.* **2023**, *9*, eadf6152.
[26] I. Park, C. Kim, R. Kim, N. Li, J. Lee, O. K. Kwon, B. Choi, T. N. Ng, D.-S. Leem, *Adv. Opt. Mater.* **2022**, *10*, 2200747.
[27] R. Englman, J. Jortner, *Mol. Phys.* **1970**, *18*, 145.
[28] J. Benduhn, K. Tvingstedt, F. Piersimoni, S. Ullbrich, Y. Fan, M. Tropiano, K. A. McGarry, O. Zeika, M. K. Riede, C. J. Douglas, S. Barlow, S. R. Marder, D. Neher, D. Spoltore, K. Vandewal, *Nat. Energy* **2017**, *2*, 17053.
[29] M. Azzouzi, J. Yan, T. Kirchartz, K. Liu, J. Wang, H. Wu, J. Nelson, *Phys. Rev. X* **2018**, *8*, 031055.
[30] X.-K. Chen, D. Qian, Y. Wang, T. Kirchartz, W. Tress, H. Yao, J. Yuan, M. Hülsbeck, M. Zhang, Y. Zou, Y. Sun, Y. Li, J. Hou, O. Inganäs, V. Coropceanu, J.-L. Bredas, F. Gao, *Nat. Energy* **2021**, *6*, 799.
[31] I. Glowacki, J. Jung, G. Wiosna–Salyga, M. Chapran, A. Luczak, B. G. Dupont, B. Luszczynska, J. Ulanski, *Disp. Imaging* **2017**, *2*, 279.
[32] L. G. Kaake, P. F. Barbara, X. Y. Zhu, *J. Phys. Chem. Lett.* **2010**, *1*, 628.
[33] H. F. Haneef, A. M. Zeidell, O. D. Jurchescu, *J. Mater. Chem. C* **2020**, *8*, 759.
[34] A. Köhler, H. Bässler, *Electronic Processes in Organic Semiconductors: An Introduction*, Wiley, Weinheim **2015**.
[35] S. R. Forrest, *Organic Electronics: Foundations to Applications*, Oxford University Press, New York **2020**.
[36] U. Würfel, D. Neher, A. Spies, S. Albrecht, *Nat. Commun.* **2015**, *6*, 6951.
[37] T. Kirchartz, B. E. Pieters, J. Kirkpatrick, U. Rau, J. Nelson, *Phys. Rev. B* **2011**, *83*, 115209.
[38] J. Wu, J. Luke, H. K. H. Lee, P. Shakya Tuladhar, H. Cha, S.-Y. Jang, W. C. Tsoi, M. Heeney, H. Kang, K. Lee, T. Kirchartz, J.-S. Kim, J. R. Durrant, *Nat. Commun.* **2019**, *10*, 5159.
[39] B. Xiao, P. Calado, R. C. I. MacKenzie, T. Kirchartz, J. Yan, J. Nelson, *Phys. Rev. Appl.* **2020**, *14*, 024034.

© 2023 The Authors. Advanced Materials Technologies published by Wiley-VCH GmbH

[40] S. M. Hosseini, S. Wilken, B. Sun, F. Huang, S. Y. Jeong, H. Y. Woo, V. Coropceanu, S. Shoaee, *Adv. Energy Mater.* **2023**, *13*, 2203576.
[41] P. Hartnagel, S. Ravishankar, B. Klingebiel, O. Thimm, T. Kirchartz, *Adv. Energy Mater.* **2023**, *13*, 2300329.
[42] Z. M. Beiley, E. T. Hoke, R. Noriega, J. Dacuña, G. F. Burkhard, J. A. Bartelt, A. Salleo, M. F. Toney, M. D. McGehee, *Adv. Energy Mater.* **2011**, *1*, 954.
[43] O. J. Sandberg, S. Zeiske, N. Zarrabi, P. Meredith, A. Armin, *Phys. Rev. Lett.* **2020**, *124*, 128001.
[44] C. Labanti, J. Wu, J. Shin, S. Limbu, S. Yun, F. Fang, S. Y. Park, C.-J. Heo, Y. Lim, T. Choi, H.-J. Kim, H. Hong, B. Choi, K.-B. Park, J. R. Durrant, J.-S. Kim, *Nat. Commun.* **2022**, *13*, 3745.
[45] M. M. Erwin, J. McBride, A. V. Kadavanich, S. J. Rosenthal, *Thin Solid Films* **2002**, *409*, 198.
[46] R. F. Salzman, J. Xue, B. P. Rand, A. Alexander, M. E. Thompson, S. R. Forrest, *Org. Electron.* **2005**, *6*, 242.
[47] F. C. Krebs, R. B. Nyberg, M. Jørgensen, *Chem. Mater.* **2004**, *16*, 1313.
[48] M. Kielar, M. Daanoune, O. François-Martin, B. Flament, O. Dhez, A. K. Pandey, S. Chambon, R. Clerc, L. Hirsch, *Adv. Electron. Mater.* **2018**, *4*, 1700526.
[49] Q. Niu, G.-J. A. H. Wetzelaer, P. W. M. Blom, N. I. Crăciun, *Appl. Phys. Lett.* **2019**, *114*, 163301.
[50] R. A. Street, A. Krakaris, S. R. Cowan, *Adv. Funct. Mater.* **2012**, *22*, 4608.
[51] G. T. Wright, *Solid State Electron.* **1961**, *2*, 165.
[52] N. F. Mott, R. W. Gurney, *Electronic Processes in Ionic Crystals*, Clarendon Press, Oxford **1940**.
[53] J. C. Blakesley, F. A. Castro, W. Kylberg, G. F. A. Dibb, C. Arantes, R. Valaski, M. Cremona, J. S. Kim, J.-S. Kim, *Org. Electron.* **2014**, *15*, 1263.
[54] L. Onsager, *J. Chem. Phys.* **1934**, *2*, 599.
[55] C. L. Braun, *J. Chem. Phys.* **1984**, *80*, 4157.
[56] D. Liraz, N. Tessler, *Chem. Phys. Rev.* **2022**, *3*, 031305.
[57] S. A. Hawks, G. Li, Y. Yang, R. A. Street, *J. Appl. Phys.* **2014**, *116*, 074503.
[58] C. M. Proctor, M. Kuik, T.-Q. Nguyen, *Prog. Polym. Sci.* **2013**, *38*, 1941.
[59] T. M. Clarke, J. R. Durrant, *Chem. Rev.* **2010**, *110*, 6736.
[60] C. Deibel, T. Strobel, V. Dyakonov, *Adv. Mater.* **2010**, *22*, 4097.
[61] T. M. Burke, S. Sweetnam, K. Vandewal, M. D. McGehee, *Adv. Energy Mater.* **2015**, *5*, 1500123.
[62] G. F. A. Dibb, T. Kirchartz, D. Credgington, J. R. Durrant, J. Nelson, *J. Phys. Chem. Lett.* **2011**, *2*, 2407.
[63] C. Deibel, A. Wagenpfahl, *Phys. Rev. B* **2010**, *82*, 207301.
[64] D. J. Wehenkel, L. J. A. Koster, M. M. Wienk, R. A. J. Janssen, *Phys. Rev. B* **2012**, *85*, 125203.
[65] U. Würfel, L. Perdigón-Toro, J. Kurpiers, C. M. Wolff, P. Caprioglio, J. J. Rech, J. Zhu, X. Zhan, W. You, S. Shoaee, D. Neher, M. Stolterfoht, *J. Phys. Chem. Lett.* **2019**, *10*, 3473.
[66] W. Shockley, W. T. Read Jr., *Phys. Rev.* **1952**, *87*, 835.
[67] R. N. Hall, *Phys. Rev.* **1952**, *87*, 387.
[68] G. A. H. Wetzelaer, M. Kuik, H. T. Nicolai, P. W. M. Blom, *Phys. Rev. B* **2011**, *83*, 165204.
[69] M. Kuik, L. J. A. Koster, G. A. H. Wetzelaer, P. W. M. Blom, *Phys. Rev. Lett.* **2011**, *107*, 256805.
[70] R. S. Crandall, *Photoconductivity, in Hydrogenated Amorphous Silicon (Semiconductors and Semimetals)*, Ed.: J.I. Pankove, Vol. *21B*, Academic Press Inc., Cambridge **1984**, p. 245.
[71] A. Rose, *RCA Rev.* **1951**, *12*, 362.
[72] A. Rose, *Concepts in Photoconductivity and Allied Problems*, Interscience Publishers, New York **1963**.
[73] J. G. Simmons, G. W. Taylor, *Phys. Rev. B* **1971**, *4*, 502.
[74] G. Marcano, A. R. Zanatta, I. Chambouleyron, *J. Appl. Phys.* **1994**, *75*, 4662.
[75] M. Kuik, H. T. Nicolai, M. Lenes, G.-J. A. H. Wetzelaer, M. Lu, P. W. M. Blom, *Appl. Phys. Lett.* **2011**, *98*, 093301.
[76] X. Ma, H. Bin, B. T. van Gorkom, T. P. A. van der Pol, M. J. Dyson, C. H. L. Weijtens, M. Fattori, S. C. J. Meskers, A. J. J. M. van Breemen, D. Tordera, R. A. J. Janssen, G. H. Gelinck, *Adv. Mater.* **2023**, *35*, 2209598.
[77] A. Cuevas, *Energy Procedia* **2014**, *55*, 53.
[78] H. T. Nicolai, M. Kuik, G. Wetzelaer, B. de Boer, C. Campbell, C. Risko, J. L. Brédas, P. W. M. Blom, *Nat. Mater.* **2012**, *11*, 882.
[79] D. Abbaszadeh, A. Kunz, N. B. Kotadiya, A. Mondal, D. Andrienko, J. J. Michels, G.-J. A. H. Wetzelaer, P. W. M. Blom, *Chem. Mater.* **2019**, *31*, 6380.
[80] B. van der Zee, Y. Li, G.-J. A. H. Wetzelaer, P. W. M. Blom, *Adv. Electron. Mater.* **2022**, *8*, 2101261.
[81] N. B. Kotadiya, A. Mondal, P. W. M. Blom, D. Andrienko, G.-J. A. H. Wetzelaer, *Nat. Mater.* **2019**, *18*, 1182.
[82] M. Diethelm, M. Bauer, W.-H. Hu, C. Vael, S. Jenatsch, P. W. M. Blom, F. Nüesch, R. Hany, *Adv. Funct. Mater.* **2022**, *32*, 2106185.
[83] G. Zuo, M. Linares, T. Upreti, M. Kemerink, *Nat. Mater.* **2019**, *18*, 588.
[84] M. Nikolka, K. Broch, J. Armitage, D. Hanifi, P. J. Nowack, D. Venkateshvaran, A. Sadhanala, J. Saska, M. Mascal, S.-H. Jung, J. K. Lee, I. McCulloch, A. Salleo, H. Sirringhaus, *Nat. Commun.* **2019**, *10*, 2122.
[85] Q. Liu, S. Zeiske, X. Jiang, D. Desta, S. Mertens, S. Gielen, R. Shanivarasanthe, H.-G. Boyen, A. Armin, K. Vandewal, *Nat. Commun.* **2022**, *13*, 5194.
[86] Y. Song, Z. Zhong, P. He, G. Yu, Q. Xue, L. Lan, F. Huang, *Adv. Mater.* **2022**, *34*, 2201827.
[87] H. Lin, B. Xu, J. Wang, X. Yu, X. Du, C.-J. Zheng, S. Tao, *ACS Appl. Mater. Interfaces* **2022**, *14*, 34891.
[88] R. H. Parmenter, W. Ruppel, *J. Appl. Phys.* **1959**, *30*, 1548.
[89] L. M. Rosenberg, M. A. Lampert, *J. Appl. Phys.* **1970**, *41*, 508.
[90] G.-J. A. H. Wetzelaer, N. J. Van der Kaap, L. J. A. Koster, P. W. M. Blom, *Adv. Energy Mater.* **2013**, *3*, 1130.
[91] B. G. Martin, *J. Appl. Phys.* **1994**, *75*, 4539.
[92] G. Zuo, Z. Li, O. Andersson, H. Abdalla, E. Wang, M. Kemerink, *J. Phys. Chem. C* **2017**, *121*, 7767.
[93] C. v Berkel, M. J. Powell, A. R. Franklin, I. D. French, *J. Appl. Phys.* **1993**, *73*, 5264.
[94] P. De Bruyn, A. H. P. Van Rest, G. A. H. Wetzelaer, D. M. de Leeuw, P. W. M. Blom, *Phys. Rev. Lett.* **2013**, *111*, 186801.
[95] G.-J. A. H. Wetzelaer, P. W. M. Blom, *NPG Asia Mater.* **2014**, *6*, e110.
[96] A. Armin, N. Zarrabi, O. J. Sandberg, C. Kaiser, S. Zeiske, W. Li, P. Meredith, *Adv. Energy Mater.* **2020**, *10*, 2001828.
[97] O. J. Sandberg, C. Kaiser, S. Zeiske, N. Zarrabi, S. Gielen, W. Maes, K. Vandewal, P. Meredith, A. Armin, *Nat. Photonics* **2023**, *17*, 368.
[98] T. Walter, R. Herberholz, C. Müller, H. W. Schock, *J. Appl. Phys.* **1996**, *80*, 4411.
[99] L. Xu, J. Wang, J. W. P. Hsu, *Phys. Rev. Appl.* **2016**, *6*, 064020.
[100] E. Von Hauff, *J. Phys. Chem. C* **2019**, *123*, 11329.
[101] M. M. Mandoc, W. Veurman, L. J. A. Koster, B. de Boer, P. W. M. Blom, *Adv. Funct. Mater.* **2007**, *17*, 2167.
[102] S. Ryu, N. Y. Ha, Y. H. Ahn, J.-Y. Park, S. Lee, *Sci. Rep.* **2021**, *11*, 16781.
[103] V. V. Brus, N. Schopp, S.-J. Ko, J. Vollbrecht, J. Lee, A. Karki, G. C. Bazan, T.-Q. Nguyen, *Adv. Energy Mater.* **2021**, *11*, 2003091.
[104] T. Kirchartz, F. Deledalle, P. S. Tuladhar, J. R. Durrant, J. Nelson, *J. Phys. Chem. Lett.* **2013**, *4*, 2371.
[105] S. Zeiske, O. J. Sandberg, N. Zarrabi, W. Li, P. Meredith, A. Armin, *Nat. Commun.* **2021**, *12*, 3603.
[106] V. D. Mihailetchi, J. Wildeman, P. W. M. Blom, *Phys. Rev. Lett.* **2005**, *94*, 126602.

© 2023 The Authors. Advanced Materials Technologies published by Wiley-VCH GmbH

2365709x, 2023, 16, Downloaded from https://onlinelibrary.wiley.com/doi/10.1002/admt.202300234 by Technical University Eindhoven, Wiley Online Library on [06/09/2023]. See the Terms and Conditions (https://onlinelibrary.wiley.com/terms-and-conditions) on Wiley Online Library for rules of use; OA articles are governed by the applicable Creative Commons License

[107] A. Ligthart, G. H. Gelinck, S. C. J. Meskers, *Org. Electron.* **2016**, *34*, 218.
[108] D. Liraz, P. Cheng, Y. Yang, N. Tessler, *J. Appl. Phys.* **2022**, *131*, 135501.
[109] C. Fuentes-Hernandez, W.-F. Chou, T. M. Khan, L. Diniz, J. Lukens, F. A. Larrain, V. A. Rodriguez-Toro, B. Kippelen, *Science* **2020**, *370*, 698.
[110] Y. Park, C. Fuentes-Hernandez, K. Kim, W.-F. Chou, F. A. Larrain, S. Graham, O. N. Pierron, B. Kippelen, *Sci. Adv.* **2021**, *7*, eabj6565.
[111] P. Hartnagel, T. Kirchartz, *Adv Theory Simul* **2020**, *3*, 2000116.
[112] R. A. Street, *Adv. Mater.* **2016**, *28*, 3814.
[113] R. A. Street, K. W. Song, J. E. Northrup, S. Cowan, *Phys. Rev. B* **2011**, *83*, 165207.
[114] N. Zarrabi, O. J. Sandberg, S. Zeiske, W. Li, D. B. Riley, P. Meredith, A. Armin, *Nat. Commun.* **2020**, *11*, 5567.
[115] C. Kaiser, S. Zeiske, P. Meredith, A. Armin, *Adv. Opt. Mater.* **2020**, *8*, 1901542.
[116] S. Zeiske, C. Kaiser, P. Meredith, A. Armin, *ACS Photonics* **2020**, *7*, 256.
[117] F. Urbach, *Phys. Rev.* **1953**, *92*, 1324.
[118] C. Kaiser, O. J. Sandberg, N. Zarrabi, W. Li, P. Meredith, A. Armin, *Nat. Commun.* **2021**, *12*, 3988.
[119] R. Ollearo, J. Wang, M. J. Dyson, C. H. L. Weijtens, M. Fattori, B. T. van Gorkom, A. J. J. M. van Breemen, S. C. J. Meskers, R. A. J. Janssen, G. H. Gelinck, *Nat. Commun.* **2021**, *12*, 7277.
[120] U. Rau, *Phys. Rev. B* **2007**, *76*, 085303
[121] D. B. Riley, O. J. Sandberg, N. M. Wilson, W. Li, S. Zeiske, N. Zarrabi, P. Meredith, R. Österbacka, A. Armin, *Phys. Rev. Appl.* **2021**, *15*, 064035.
[122] D. W. Miller, G. E. Eperon, E. T. Roe, C. W. Warren, H. J. Snaith, M. C. Lonergan, *Appl. Phys. Lett.* **2016**, *109*, 153902.
[123] C. M. Sutter-Fella, D. W. Miller, Q. P. Ngo, E. T. Roe, F. M. Toma, I. D. Sharp, M. C. Lonergan, A. Javey, *ACS Energy Lett.* **2017**, *2*, 709.
[124] B. T. van Gorkom, T. P. A. van der Pol, K. Datta, M. M. Wienk, R. A. J. Janssen, *Nat. Commun.* **2022**, *13*, 349.
[125] J. Melskens, M. Schouten, R. Santbergen, M. Fischer, R. Vasudevan, D. J. van der Vlies, R. J. V. Quax, S. G. M. Heirman, K. Jäger, V. Demontis, M. Zeman, A. H. M. Smets, *Sol. Energy Mater. Sol. Cells* **2014**, *129*, 70.
[126] A. Armin, M. Hambsch, I. K. Kim, P. L. Burn, P. Meredith, E. B. Namdas, *Laser Photonics Rev.* **2014**, *8*, 924.
[127] P. Peumans, V. Bulović, S. R. Forrest, *Appl. Phys. Lett.* **2000**, *76*, 3855.
[128] D. Yang, D. Ma, *J. Mater. Chem. C* **2013**, *1*, 2054.
[129] K. Kato, H. Susumu, K. Kawano, A. Kozen, *IEICE Trans. Electron.* **1993**, *E76-C*, 214.
[130] K. Kato, *IEEE Trans. Microwave Theory Tech.* **1999**, *47*, 1265.
[131] M. Kielar, O. Dhez, G. Pecastaings, A. Curutchet, L. Hirsch, *Sci. Rep.* **2016**, *6*, 39201.
[132] F. Wang, X. Zou, M. Xu, H. Wang, H. Wang, H. Guo, J. Guo, P. Wang, M. Peng, Z. Wang, Y. Wang, J. Miao, F. Chen, J. Wang, X. Chen, A. Pan, C. Shan, L. Liao, W. Hu, *Adv. Sci.* **2021**, *8*, 2100569.
[133] F. Arca, S. F. Tedde, M. Sramek, J. Rauh, P. Lugli, O. Hayden, *Sci. Rep.* **2013**, *3*, 1324.
[134] H.-J. Yun, M. C. Hwang, S. M. Park, R. Kim, D. S. Chung, Y.-H. Kim, S.-K. Kwon, *ACS Appl. Mater. Interfaces* **2013**, *5*, 6045.
[135] Z. Li, C. R. McNeill, *J. Appl. Phys.* **2011**, *109*, 074513.
[136] C. R. McNeill, I. Hwang, N. C. Greenham, *J. Appl. Phys.* **2009**, *106*, 024507.
[137] Z. Li, G. Lakhwani, N. C. Greenham, C. R. McNeill, *J. Appl. Phys.* **2013**, *114*, 034502.
[138] R. C. I. MacKenzie, C. G. Shuttle, G. F. Dibb, N. Treat, E. von Hauff, M. J. Robb, C. J. Hawker, M. L. Chabinyc, J. Nelson, *J. Phys. Chem. C* **2013**, *117*, 12407.
[139] E. S. Zaus, S. Tedde, J. Fürst, D. Henseler, G. H. Döhler, *J. Appl. Phys.* **2007**, *101*, 044501.
[140] B. V. Popescu, D. H. Popescu, P. Lugli, S. Locci, F. Arca, S. F. Tedde, M. Sramek, O. Hayden, *IEEE Trans. Electron Devices* **2013**, *60*, 1975.
[141] I. Hwang, C. R. McNeill, N. C. Greenham, *J. Appl. Phys.* **2009**, *106*, 094506.
[142] R. A. Street, *Phys. Rev. B* **2011**, *84*, 075208.
[143] R. Ollearo, A. Caiazzo, J. Li, M. Fattori, A. J. van Breemen, M. M. Wienk, G. H. Gelinck, R. A. Janssen, *Adv. Mater.* **2022**, *34*, 2205261.
[144] A. J. J. M. van Breemen, R. Ollearo, S. Shanmugam, B. Peeters, L. C. J. M. Peters, R. L. van de Ketterij, I. Katsouras, H. B. Akkerman, C. H. Frijters, F. Di Giacomo, S. Veenstra, R. Andriessen, R. A. J. Janssen, E. A. Meulenkamp, G. H. Gelinck, *Nat. Electron.* **2021**, *4*, 818.
[145] L. Tzabari, N. Tessler, *J. Appl. Phys.* **2011**, *109*, 064501.
[146] Y. Yao, Y. Liang, V. Shrotriya, S. Xiao, L. Yu, Y. Yang, *Adv. Mater.* **2007**, *19*, 3979.
[147] L. Zhang, T. Yang, L. Shen, Y. Fang, L. Dang, N. Zhou, X. Guo, Z. Hong, Y. Yang, H. Wu, J. Huang, Y. Liang, *Adv. Mater.* **2015**, *27*, 6496.
[148] S. Xiong, L. Li, F. Qin, L. Mao, B. Luo, Y. Jiang, Z. Li, J. Huang, Y. Zhou, *ACS Appl. Mater. Interfaces* **2017**, *9*, 9176.
[149] Z. Wu, N. Li, N. Eedugurala, J. D. Azoulay, D.-S. Leem, T. N. Ng, *Npj Flex Electron.* **2020**, *4*, 6.
[150] Z. Huang, Z. Zhong, F. Peng, L. Ying, G. Yu, F. Huang, Y. Cao, *ACS Appl. Mater. Interfaces* **2021**, *13*, 1027.
[151] J. Huang, J. Lee, H. Nakayama, M. Schrock, D. X. Cao, K. Cho, G. C. Bazan, T.-Q. Nguyen, *ACS Nano* **2021**, *15*, 1753.
[152] W. Yang, W. Qiu, E. Georgitzikis, E. Simoen, J. Serron, J. Lee, I. Lieberman, D. Cheyns, P. Malinowski, J. Genoe, H. Chen, P. Heremans, *ACS Appl. Mater. Interfaces* **2021**, *13*, 16766.
[153] S. Xiong, J. Li, J. Peng, X. Dong, F. Qin, W. Wang, L. Sun, Y. Xu, Q. Lin, Y. Zhou, *Adv. Opt. Mater.* **2022**, *10*, 2101837.
[154] P. Jacoutot, A. D. Scaccabarozzi, T. Zhang, Z. Qiao, F. Aniés, M. Neophytou, H. Bristow, R. Kumar, M. Moser, A. D. Nega, A. Schiza, A. Dimitrakopoulou-Strauss, V. G. Gregoriou, T. D. Anthopoulos, M. Heeney, I. McCulloch, A. A. Bakulin, C. L. Chochos, N. Gasparini, *Small* **2022**, *18*, 2200580.
[155] M. Ramuz, L. Bürgi, C. Winnewisser, P. Seitz, *Org. Electron.* **2008**, *9*, 369.
[156] X. Gong, M. Tong, Y. Xia, W. Cai, J. S. Moon, Y. Cao, G. Yu, C.-L. Shieh, B. Nilsson, A. J. Heeger, *Science* **2009**, *325*, 1665.
[157] E. Saracco, B. Bouthinon, J.-M. Verilhac, C. Celle, N. Chevalier, D. Mariolle, O. Dhez, J.-P. Simonato, *Adv. Mater.* **2013**, *25*, 6534.
[158] X. Zhou, D. Yang, D. Ma, *Adv. Opt. Mater.* **2015**, *3*, 1570.
[159] A. Pierre, I. Deckman, P. B. Lechêne, A. C. Arias, *Adv. Mater.* **2015**, *27*, 6411.
[160] M. G. Han, K.-B. Park, X. Bulliard, G. H. Lee, S. Yun, D.-S. Leem, C.-J. Heo, T. Yagi, R. Sakurai, T. Ro, S.-J. Lim, S. Sul, K. Na, J. Ahn, Y. W. Jin, S. Lee, *ACS Appl. Mater. Interfaces* **2016**, *8*, 26143.
[161] S. H. Eom, S. Y. Nam, H. J. Do, J. Lee, S. Jeon, T. J. Shin, I. H. Jung, S. C. Yoon, C. Lee, *Polym. Chem.* **2017**, *8*, 3612.
[162] Z. Tang, Z. Ma, A. Sánchez-Díaz, S. Ullbrich, Y. Liu, B. Siegmund, A. Mischok, K. Leo, M. Campoy-Quiles, W. Li, K. Vandewal, *Adv. Mater.* **2017**, *29*, 1702184.
[163] Y. Wei, Z. Ren, A. Zhang, P. Mao, H. Li, X. Zhong, W. Li, S. Yang, J. Wang, *Adv. Funct. Mater.* **2018**, *28*, 1706690.
[164] L. Xiao, S. Chen, X. Chen, X. Peng, Y. Cao, X. Zhu, *J. Mater. Chem. C* **2018**, *6*, 3341.
[165] C. M. Benavides, P. Murto, C. L. Chochos, V. G. Gregoriou, A. Avgeropoulos, X. Xu, K. Bini, A. Sharma, M. R. Andersson, O.

 © 2023 The Authors. Advanced Materials Technologies published by Wiley-VCH GmbH

2365709x, 2023, 16, Downloaded from https://onlinelibrary.wiley.com/doi/10.1002/admt.202300234 by Technical University Eindhoven, Wiley Online Library on [06/09/2023]. See the Terms and Conditions (https://onlinelibrary.wiley.com/terms-and-conditions) on Wiley Online Library for rules of use; OA articles are governed by the applicable Creative Commons License

Schmidt, C. J. Brabec, E. Wang, S. F. Tedde, *ACS Appl. Mater. Interfaces* **2018**, *10*, 12937.
[166] Z. Zhong, K. Li, J. Zhang, L. Ying, R. Xie, G. Yu, F. Huang, Y. Cao, *ACS Appl. Mater. Interfaces* **2019**, *11*, 14208.
[167] G. H. Lee, X. Bulliard, S. Yun, D.-S. Leem, K.-B. Park, K.-H. Lee, C.-J. Heo, I.-S. Jung, J.-H. Kim, Y. S. Choi, S.-J. Lim, Y. W. Jin, *Opt. Express* **2019**, *27*, 25410.
[168] C.-C. Lee, R. Estrada, Y.-Z. Li, S. Biring, N. R. A. Amin, M.-Z. Li, S.-W. Liu, K.-T. Wong, *Adv. Opt. Mater.* **2020**, *8*, 2000519.
[169] J. Kang, J. Kim, H. Ham, H. Ahn, S. Y. Lim, H. M. Kim, I.-N. Kang, I. H. Jung, *Adv. Opt. Mater.* **2020**, *8*, 2001038.
[170] K. Xia, Y. Li, Y. Wang, L. Portilla, V. Pecunia, *Adv. Opt. Mater.* **2020**, *8*, 1902056.

Xiao Ma received his master's degree from the Sichuan University in China in 2018 on Advanced Energy Materials and Devices. In September 2018, he began his Ph.D. study at Eindhoven University of Technology, The Netherlands, where he worked on organic bulk heterojunction photodetectors. On May 22, 2023 he received his Ph.D. after successfully defending his thesis entitled "The Origin of Dark Current and Trap States in Organic Photodiodes."

René A. J. Janssen is a professor of chemistry and physics at TU/e, The Netherlands. His current research focuses on molecular organic and hybrid semiconductors for optoelectronic applications, energy conversion, and energy storage. The work combines synthetic chemistry with optical spectroscopy, morphological characterization and the design, and fabrication and characterization of functional devices.

Gerwin H. Gelinck is a professor of applied physics at TU/e, The Netherlands. He joined Philips Research as a Senior Scientist in 1998. From 2002 to 2006, he was the Chief Scientist of Polymer Vision, a rollable display company. Since 2007, he works at Holst Centre. His research interests include novel solution-processed semiconductors for applications in thin-film transistors, actuators, and photodiodes.

© 2023 The Authors. Advanced Materials Technologies published by Wiley-VCH GmbH

2365709x, 2023, 16, Downloaded from https://onlinelibrary.wiley.com/doi/10.1002/admt.202300234 by Technical University Eindhoven, Wiley Online Library on [06/09/2023]. See the Terms and Conditions (https://onlinelibrary.wiley.com/terms-and-conditions) on Wiley Online Library for rules of use; OA articles are governed by the applicable Creative Commons License